AD-A128 783 CALCULATION OF WAVE RESISTANCE AND SINKAGE BY RANKINE-SOURCE METHOD PREDI..(U) IOWA INST OF HYDRAULIC RESEARCH IOWA CITY K MORI MAY 83 IIHR-262 1/1

UNCLASSIFIED N00014-82-K-0016 F/G 20/4 NL

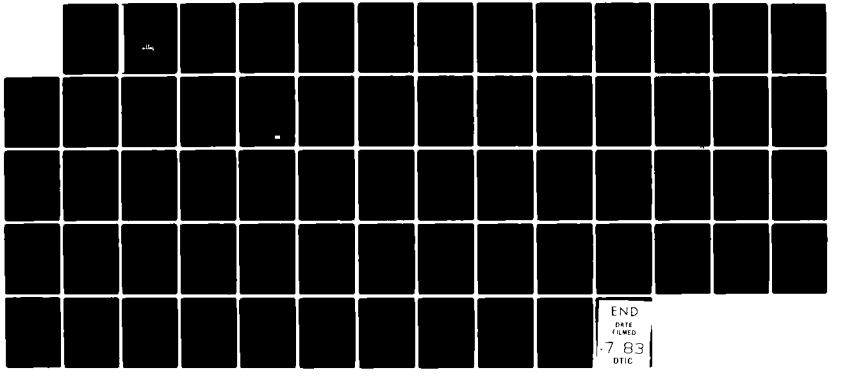

END
DATE FILMED
7 83
DTIC

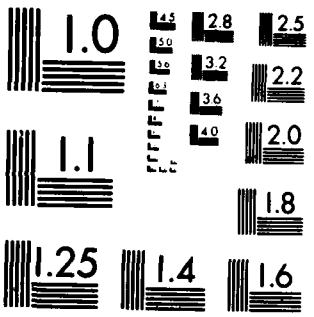

(12)

A. CALCULATION OF WAVE RESISTANCE AND SINKAGE BY RANKINE-SOURCE METHOD

B. PREDICTION OF 2-D NEAR WAKE FLOW BY MAKING USE OF TIME-DEPENDENT VORTICITY TRANSPORT EQUATION

C. FREE-SURFACE BOUNDARY LAYER AND NECKLACE VORTEX FORMATION

Progress Reports by
KAZUHIRO MORI

Sponsored by
General Hydromechanics Research Program
of the Naval Sea Systems Command
David W. Taylor Naval Ship Research and Development Center
Contracts Nos. N00014-82-K0016 and N0014-82K0200

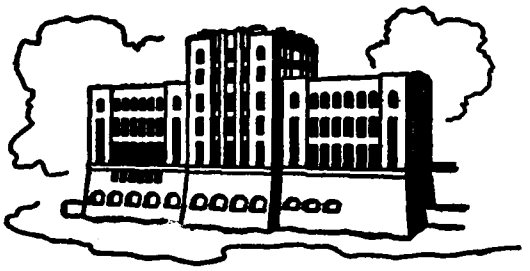

IIHR Report No. 262
Iowa Institute of Hydraulic Research
The University of Iowa
Iowa City, Iowa 52242
May 1983
Approved for public release; distribution unlimited

SECURITY CLASSIFICATION OF THIS PAGE (When Data Entered)

REPORT DOCUMENTATION PAGE		READ INSTRUCTIONS BEFORE COMPLETING FORM
1. REPORT NUMBER 262	2. GOVT ACCESSION NO. AD-A128783	3. RECIPIENT'S CATALOG NUMBER
4. TITLE (and Subtitle) Contributions on - A) Calculation of Wave Resistance and Sinkage by Rankine-Source Method; B) Prediction of 2D Near Wake Flow by Making use of Time-Dependent Vorticity Transport Equation; C) Free-Surface Boundary Layer and Necklace Vortex Formation.		5. TYPE OF REPORT & PERIOD COVERED Interim Report 6. PERFORMING ORG. REPORT NUMBER 262
7. AUTHOR(s) Kazuhiro Mori		8. CONTRACT OR GRANT NUMBER(s) N00014-82-K-0016 N00014-82-K-0200
9. PERFORMING ORGANIZATION NAME AND ADDRESS Institute of Hydraulic Research The University of Iowa Iowa City, Iowa 52242		10. PROGRAM ELEMENT, PROJECT, TASK AREA & WORK UNIT NUMBERS
11. CONTROLLING OFFICE NAME AND ADDRESS Code 1505 David W. Taylor Naval Ship R. & D. Center Bethesda, MD 20084		12. REPORT DATE May 1983 13. NUMBER OF PAGES
14. MONITORING AGENCY NAME & ADDRESS(if different from Controlling Office)		15. SECURITY CLASS. (of this Report) Unclassified 15a. DECLASSIFICATION/DOWNGRADING SCHEDULE

16. DISTRIBUTION STATEMENT (of this Report)

Approved for public release, distribution unlimited

17. DISTRIBUTION STATEMENT (of the abstract entered in Block 20, if different from Report)

18. SUPPLEMENTARY NOTES

19. KEY WORDS (Continue on reverse side if necessary and identify by block number)

Ship wave resistance, ship wakes, bow phenomena

20. ABSTRACT (Continue on reverse side if necessary and identify by block number)

A. The flow about a wavemaking ship form is treated in terms of source distributions on the wetted hull and the free surface, with the simple source potential serving as the Green function. The free-surface boundary condition is linearized based on the double-hull flow, and the hull surface condition is approximately satisfied by the double hull potential. The equations are discretized by finite-difference methods and solved iteratively. Results are given for Inuid model M-21 and a Wigley parabolic ship form. (OVER)

-> cont

DD FORM 1 JAN 73 1473 EDITION OF 1 NOV 65 IS OBSOLETE
S/N 0102-014-6601 |

SECURITY CLASSIFICATION OF THIS PAGE (When Data Entered)

B. The vorticity-transport equation is applied to predict near-wake flows of shiplike bodies, with initial or boundary values given by an upstream boundary-layer calculation. Vorticity transport is calculated by a finite-difference time-marching method. The k-e model is applied for closure of the turbulence equations. Near wakes of a flat plate and two elliptic cylinders are calculated.

C. A shear layer, or free-surface boundary layer may develop under a free surface with significant curvature due to a zero-free-stress boundary condition. Equations for predicting this development are presented. A weak vorticity generated by this mechanism may be amplified by vortex stretching as the flow approaches a ship bow. This theory can explain the formation of the so-called necklace vortex around the bow. A simple calculation for the case of a vertical circular cylinder demonstrates that the formation of a necklace vortex can be prevented by a bulbous bow.

A. CALCULATION OF WAVE RESISTANCE AND SINKAGE BY RANKINE-SOURCE METHOD

B. PREDICTION OF 2-D NEAR WAKE FLOW BY MAKING USE OF TIME-DEPENDENT VORTICITY TRANSPORT EQUATION

C. FREE-SURFACE BOUNDARY LAYER AND NECKLACE VORTEX FORMATION

Progress Reports by
KAZUHIRO MORI

Sponsored by
General Hydromechanics Research Program
of the Naval Sea Systems Command
David W. Taylor Naval Ship Research and Development Center
Contracts Nos. N00014-82-K0016 and N0014-82K0200

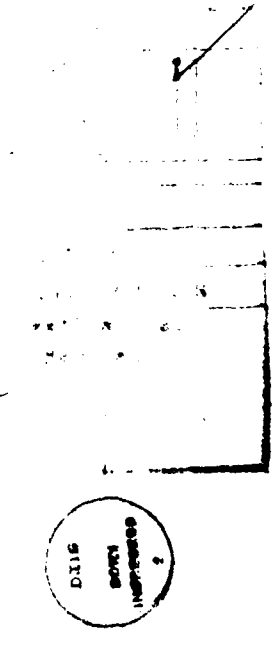

IIHR Report No. 262
Iowa Institute of Hydraulic Research
The University of Iowa
Iowa City, Iowa 52242
May 1983
Approved for public release; distribution unlimited

A. CALCULATION OF WAVE RESISTANCE AND SINKAGE BY RANKINE-SOURCE METHOD

B. PREDICTION OF 2-D NEAR WAKE FLOW BY MAKING USE OF TIME-DEPENDENT VORTICITY TRANSPORT EQUATION

C. FREE-SURFACE BOUNDARY LAYER AND NECKLACE VORTEX FORMATION

Progress Reports by

KAZUHIRO MORI

Sponsored by
General Hydromechanics Research Program
of the Naval Sea Systems Command
David W. Taylor Naval Ship Research and Development Center
Contracts Nos. N00014-82-K0016 and N0014-82K0200

IIHR Report No. 262

Iowa Institute of Hydraulic Research
The University of Iowa
Iowa City, Iowa 52242

October 1982

Acknowledgments

The present work was supported in part by the General Hydrodynamics Research Program of the David W. Taylor Naval Ship Research and Development Center under the Contract Nos. N00014-82-K0016 and N00014-82-K0200, which are gratefully acknowledged.

The author is grateful to Professors L. Landweber and V.C. Patel at IIHR, who are the principal investigators of the contracts, for their valuable discussions and suggestions. Thanks should be extended to Mr. K. Murata, Mr. N. Ito and Mr. C.J. Tang who are involved in the subjects A, B and C respectively.

The stay at IIHR was really superb. Especially its international academic atmosphere was so pleasant. The author wishes to express his cordial thanks, lastly but this does not mean less, to Professor J.F. Kennedy, the director of IIHR, and others of the staff of IIHR for their warm hospitality.

A. Calculation of Wave Resistance and Sinkage by Rankine-Source Method

1. Introduction

The Rankine source was used first by Gadd [1] for the free-surface flow problem. Later Dawson derived a more elegant formula and presented many numerical results which may be considered a milestone in ship hydrodynamics [2,3].

One of the significant advantages of the method is its generality and the simple form of the Green function. When the double-hull linearized free-surface condition is used, it can be extended to the viscous flow problem (Mori & Nishimoto [4]). Not only the wave resistance but also the moment and the force acting on a ship hull can be calculated. It enables us to attain our final goal to calculate the wave resistance of an unrestrained ship form, including viscous effects.

In the present interim report, calculations are limited to the case of potential flow under the restrained condition. This is because there are still several points which should be clarified in the numerical techniques. The inclusion of viscosity and the iterative calculation to realize the trim- and sinkage-free condition are left for the second half of the present work.

2. Basic equations

Let $\phi(x,y,z)$ be the perturbation velocity potential at $P(x,y,z)$(see Fig. 1 for definitions). By Green's theorem, ϕ can be expressed in the form

$$4\pi\phi(P) = -\iint_{S_H} \sigma_H\left(\frac{1}{r} + \frac{1}{r'}\right)dS - \iint_{S_F} \sigma_F \frac{1}{r}\, dS + 4\pi\,\phi_\infty, \tag{1}$$

where S_H denotes the hull surface, S_F the free surface, σ_H a source distribution over S_H, and σ_F a source distribution over S_F, (see Appendix).

$$\begin{aligned} r^2 &= (x - x')^2 + (y - y')^2 + (z - z')^2 \\ r'^2 &= (x - x')^2 + (y - y')^2 + (z + z')^2, \end{aligned} \tag{2}$$

(x,y,z) are the coordinates of a fixed point P, (x',y',z') those of the integration points. ϕ_∞ is the contribution from the integration over the far-field surface S_0, given by

$$4\pi\phi_\infty = \iint_{\Sigma_3} \{\phi \frac{\partial}{\partial x}(\frac{1}{r} + \frac{1}{r'}) - (\frac{1}{r} + \frac{1}{r'}) \frac{\partial\phi}{\partial x}\} dS. \tag{3}$$

In the domain of V_0, which is partially surrounded by S_0 (see Fig. 1), we can assume that the velocity potential ϕ satisfies the linearized free-surface condition

$$K_0 \frac{\partial\phi'}{\partial z} + \frac{\partial^2\phi'}{\partial x^2} = 0, \tag{4}$$

where $K_0 = U^2/g$, g is the gravity acceleration, and U is the ship speed. By making use of the Havelock Green function G which satisfies the linearized free-surface condition, application of Green's formula gives

$$0 = -\frac{1}{K_0} \int_{L_0} (\phi' \frac{\partial G}{\partial x'} - G \frac{\partial\phi'}{\partial x'}) dy' + \iint_{S_0} (\phi' \frac{\partial G}{\partial x'} - G \frac{\partial\phi'}{\partial x'}) dS, \tag{5}$$

where L_0 is the intersecton of S_0 and the free surface.

Because ϕ' and $\partial\phi'/\partial x$ should be continuous on S_0, the addition of Eq. (5) to Eq. (3) yields

$$4\pi\phi_\infty = \frac{1}{K_0} \int_{L_0} (\phi' \frac{\partial G}{\partial x'} - G \frac{\partial\phi'}{\partial x'}) dy' - \iint_{S_0} (\phi' \frac{\partial H}{\partial x'} - H \frac{\partial\phi'}{\partial x'}) dS, \tag{6}$$

where

$$H = G + (\frac{1}{r} + \frac{1}{r'}). \tag{7}$$

Due to the exponential decay of H in the depthwise directiion, the integration over S_0 may be limited close to the free surface.

Eq. (1) has three unknowns; σ_H, σ_F and ϕ'. They can be determined so that ϕ satisfies the free-surface condition, the hull-surface condition and an additional condition on S_0. This is accomplished iteratively. We write the velocity in the form

$$\mathbf{q} = \mathbf{q}_0 + \nabla\phi_w, \tag{8}$$

where

$$\mathbf{q}_0 = iU + \nabla\phi_0 + \mathbf{q}_v, \tag{9}$$

and

$$\phi_0 = -\frac{1}{4\pi} \iint_{S_H} \sigma_H \left(\frac{1}{r} + \frac{1}{r'}\right) dS \tag{10}$$

$$\phi_w = -\frac{1}{4\pi} \iint_{S_F} \sigma_F \frac{1}{r}\, dS + \phi_\infty \tag{11}$$

Here $\mathbf{i}$ is the unit vector in the x-direction, and $\mathbf{q}_v$ a viscous velocity vector.

At first, we determine σ_H in order to satisfy the hull-surface condition for a given ϕ_w. At the first iteration, σ_F and ϕ_∞ are assumed zero. Thus $\mathbf{q}_0$, at the first iteration, gives the double-hull flow itself. Then σ_F is determined so as to satisfy the free-surface condition and a proper downstream condition imposed on S_0.

The free-surface condition, which is linearized based on the flow field of $\mathbf{q}_0$, is

$$q_0(q_0\phi_{w\ell})_\ell + q_0(q_{0x}\phi_{wx} + q_{0y}\phi_{wy}) + g\phi_{wz} = -q_0^2 q_{0\ell}, \quad \text{on } z = 0 \tag{12}$$

where $q_0 = |\mathbf{q}_0|_{z=0}$, and subscripts ℓ, x and y imply differentiation with respect to the indicated variables. Here ℓ denotes arclength along a streamline on $z = 0$.

The condition imposed on S_0 is that ϕ' must be matched with a solution of the Laplace equation which satisfies the linearized free-surface condition and the radiation condition. In the present calculation, however, ϕ_∞ is neglected by choosing the computing domain and the finite-difference scheme properly according to the pilot computations given in [4].

The transformation of Eq. (12) into a finite-difference equation provides a set of simultaneous equations for the unknown variable σ_F. Its precise expression can be found in [4].

Once the velocity potential is determined, the pressure on the hull is given by

$$p = \frac{1}{2}\rho\,(U^2 - |\mathbf{q}|^2) - \rho g \delta H, \tag{13}$$

where $\mathbf{q}$ is the total velocity vector, ρ is the density of fluid, and δH the head loss whose gradient is given by

$$g\nabla\delta H = \boldsymbol{\omega} \times \mathbf{q} - \nu\nabla^2\mathbf{q}, \tag{14}$$

where $\boldsymbol{\omega}$ is the vorticity vector and ν is the kinematic viscosity. Then, the pressure resistance, R_p, the sinkage force, R_s, and the trim-by-stern moment, M_t, are given as follows:

$$\begin{aligned} R_p &= -\iint_{S_H} p n_x \, dS, \qquad R_s = \iint_{S_H} p n_z \, dS, \\ M_t &= \iint_{S_H} p\{n_z(x - x_0) - n_x(z - z_0)\}\, dS, \end{aligned} \tag{15}$$

where (x_0, z_0) are the coordinates of the center of buoyancy, and (n_x, n_z) are the x- and z-components of the unit outward normal vector on S_H.

3. Numerical calculation and discussions

Two ships are chosen for the present calculation; an Inuid model M-21 [5] and the Wigley parabolic model whose principal dimensions are shown in Table 1. The calculations are limited to the inviscid case and the first iteration is carried out. Because M-21 is a model generated by the streamline tracing method, σ_H is exactly known, thus avoiding some numerical errors.

Fig. 2 shows the discretization of the free surface for M-21. For the present calculation, the computing domain is chosen as $-1.5 < 2x/L < 5.0$ and $0 < 2x/L < 4.5$, where L is the ship length.

The first derivatives appearing on the l.h.s. of Eq. (12) are approximated by

$$F_i' = \frac{1}{6h}\,(-F_{i-3} + 6F_{i-2} - 15F_{i-1} + 10F_i), \tag{16}$$

where h is the grid size, while those on the r.h.s. (knowns) are obtained by a simple centered difference. Eq. (17) is the form which keeps terms up to the fourth derivatives in the Taylor expansion but drops the third. It has been determined in [4] that the finite difference of Eq. (17) is better than other forms; it avoids downstream reflection and dampens waves, making it possible to satisfy the radiation condition.

The upstream condition is satisfied by requiring that the perturbation velocity ϕ_w be zero on the three upstream columns of panels (shaded in Fig. 2).

Fig. 3 shows the resulting free-surface source distribution along the 2nd and 3rd rows of panels (j = 2,3). For comparison, the results obtained by changing the computing domain from $-1.5 < 2x/L < 5.0$ to $-1.5 < 2x/L < 3.0$, are also shown. The results are quite similar. This does not always guarantee the exact satisfaction of the radiation condition, but it can be safely concluded that the truncation of the computing domain does not affect the results greatly if the selected range extends at least two ship lengths upstream and downstream from the ship form and the finite difference procedure is properly chosen.

Fig. 4a shows the comparisons of perturbation velocity components, u,v and w, in the x-, y- and z-directions respectively. The measurement is carried out at $2z/L = -0.02$ (just beneat the free surface) while the computed results are on z=o. The values of u are in good agreement except near the bow and stern. The discrepancies near the bow may be due to the approximation that ϕ_w does not satisfy the hull-surface condition, while those near the stern may be attributable to the effects of viscosity. (It is intended to include the viscous effects in subsequent calculations). The comparisons of the v- and w-components indicates the need for a slight refinement of the numerical techniques. As seen in Fig. 4b, however, the comparisons at a deeper position, $2z/L = -0.1$, shows much better agreement.

In Fig. 5 the calculated wave resistance and sinkage are compared with measured results. The measurement of resistance was carried out under the sinkage-free condition (trim-fixed). The wave resistance is obtained by subtracting the viscous resistance from the total resistance. The sinkage, 2s/L, was calculated by means of the static relation, given by

$$2s/L = \frac{2R_s}{\rho g A_w L}, \tag{17}$$

where A_w is the waterplane area.

The calculated wave resistance is smaller than that measured. This discrepancy may come mainly from the inadequate agreement in velocity (pressure) observed near the bow, especially in the u-component. Another possible reason is the neglect of sinkage in the calculation. The neglect of the viscosity is also a possible reason, for M-21 is an optimized hull and the inclusion of viscosity may increase the wave resistance.

The disagreement in the sinkage may be due to the same reasons. It should be remembered that the calculated result shown here is that of only the first iteration. Therefore, we can expect much better agreement in successive iterations where the sinkage of ship is taken into account.

In the case of the Wigley model, the hull surface is divided into 24 (lengthwise) x 5 (draftwise) panels. The computing domain is chosen as $-1.5 < 2x/L < 3.0$ and $0 < 2y/L$ 0.45, and divided into 318 panels. The calculated results of wave resistance and sinkage are compared in Fig. 6. Experimental data are those of a 4.0^m model measured at ISR [6]. The wave resistance was measured with the model restricted in sinkage, but free to trim. Dawson's results [3] are also shown in the figure.

The discrepancy, observed in the wave resistance curve at the higher speed range, may be due to the use of the double-hull linearized free-surface condition. The difference between the present results and Dawsons's may come mainly from the numerical method; he solved Eq. (1) directly to satisfy both the hull-surface condition and the free-surface condition simultaneously.

The predicted sinkage is smaller in this case also. This is probably due to the same causes as that for M-21.

Several kinds of discretization of the hull surface have been compared for the integration of pressure over the hull. These do not make any significant changes if the source distributions, σ_F and σ_H, are unchanged. A possible improvement may be obtained by making use of the Lagally theorem.

4. Concluding remarks

The Rankine source method is applied to the calculations of the wave resistance and the sinkage of the Inuid model M-21 and the Wigley model. Some improvements in numerical schemes and techniques may be still necessary, e.g. the inclusion of the far downstream contribution, to carry out a successive iteration and so on. It can be safely concluded, however, that the method works well and is useful.

The author plans to carry out extensive additional calculations, including viscous effects.

References

1) Gadd, G.E.: A Method of Computing the Flow and Surface Wave Pattern around Full Forms, Trans. of RINA, Vol. 118 (1976).

2) Dawson, C.W.: A Practical Computer Method for Solving Ship-Wave Problems, Proc. of 2nd Intern. Conf. on Numerical Ship Hydrodynamics (1977).

3) Dawson, C.W.: Calculations with XYZ Free Surface Program for Five Ship Models, Proc. of the Workshop on Ship Wave-Resistance Computations (1979).

4) Mori, K. and Nishimoto, H: Prediction of Flow Fields around Ships by Modified Rankine Source Method (1st Report) --Pilot Computations and Inviscid Case, Jour. of Soc. of Naval Arch. of Japan, Vol. 150 (1981).

5) Mori, K, Inui, T., Kajitani, H.; Analysis of Ship-Side Wave Profiles with Special Reference to Hull's Sheltering Effect, Proc. of 9th Symposium on Naval Hydrodynamics (1972).

6) ITTC Resistance Committee Report (1982).

Appendix - Derivation of Equation (1).

We consider three sub-domains of Ve, $\bar{V}_e$ and V_i which are surrounded by surfaces of S_0, $\bar{S}_0$, S_1, $\bar{S}_1$, S_2, $\bar{S}_2$, S_H, $\bar{S}_H$ and S_F (see Fig. 1). $P(x,y,z)$ is a fix point in Ve.

By applying Green's formula to the domain of Ve, $\bar{V}e$ and Vi, we have

$$4\pi\phi(p) = \iint_{S_0+S_1+S_2} \left(\phi \frac{\partial}{\partial n}\frac{1}{r} - \frac{1}{r}\frac{\partial\phi}{\partial n}\right) dS + \iint_{S_F} \left(\phi \frac{\partial}{\partial n}\frac{1}{r} - \frac{1}{r}\frac{\partial\phi}{\partial n}\right) dS + \iint_{S_H} \left(\phi \frac{\partial}{\partial n_H}\frac{1}{r} - \frac{1}{r}\frac{\partial\phi}{\partial n_H}\right) dS, \quad \text{(A-1)}$$

$$0 = \iint_{\bar{S}_0+\bar{S}_1+\bar{S}_2} \left(\bar{\phi} \frac{\partial}{\partial n}\frac{1}{r} - \frac{1}{r}\frac{\partial\bar{\phi}}{\partial n}\right) dS - \iint_{S_F} \left(\bar{\phi} \frac{\partial}{\partial n}\frac{1}{r} - \frac{1}{r}\frac{\partial\phi}{\partial n_H}\right) dS + \iint_{\bar{S}_H} \left(\bar{\phi} \frac{\partial}{\partial n_H}\frac{1}{r} - \frac{1}{r}\frac{\partial}{\partial n_H}\bar{\phi}\right) dS, \quad \text{(A-2)}$$

$$0 = -\iint_{S_H+\bar{S}_H} \left(\phi_i \frac{\partial}{\partial n_H}\frac{1}{r} - \frac{1}{r}\frac{\partial\phi_i}{\partial n_H}\right) dS \quad \text{(A-3)}$$

where $\bar{\phi}$ and ϕ_i are the velocity potential defined in $\bar{V}e$ and Vi respectively. The definition of the normals of n and n_H are shown in Fig. 1.

The integrands over S_1 and $\bar{S}_1$ vanish when the upstream condition is imposed on ϕ. Then the addition of Eqs. (A-1), (A-2) and (A-3) yields

$$\begin{aligned} 4\pi\phi(P) = {} & \iint_{S_0} \left(\phi \frac{\partial}{\partial n}\frac{1}{r} - \frac{1}{r}\frac{\partial\phi}{\partial n}\right) dS + \iint_{\bar{S}_0} \left(\bar{\phi} \frac{\partial}{\partial n}\frac{1}{r} - \frac{1}{r}\frac{\partial\bar{\phi}}{\partial n}\right) dS \\ & + \iint_{S_2} \left(\phi \frac{\partial}{\partial n}\frac{1}{r} - \frac{1}{r}\frac{\partial\phi}{\partial n}\right) dS + \iint_{\bar{S}_2} \left(\bar{\phi} \frac{\partial}{\partial n}\frac{1}{r} - \frac{1}{r}\frac{\partial\bar{\phi}}{\partial n}\right) dS \\ & + \iint_{S_F} \left\{(\phi-\bar{\phi}) \frac{\partial}{\partial n}\frac{1}{r} - \frac{1}{r}\frac{\partial}{\partial n}(\phi - \bar{\phi})\right\} dS \\ & + \iint_{S_H} \left\{(\phi-\phi_i) \frac{\partial}{\partial n_H}\frac{1}{r} - \frac{1}{r}\frac{\partial}{\partial n_H}(\phi-\phi_i)\right\} dS + \iint_{\bar{S}_H} \left\{(\bar{\phi}-\phi_i) \frac{\partial}{\partial n_H}\frac{1}{r} - \frac{1}{r}\frac{\partial}{\partial n_H}(\bar{\phi}-\phi_i)\right\} dS . \end{aligned} \quad \text{(A-4)}$$

It can be expected that the contributions from the integrations over S_2 and $\bar{S}_2$, the third and fourth terms in Eq. (A-4), may cancel each other when S_2 and $\bar{S}_2$ are taken deep enough. We assume that $\bar{\phi}$ is equal to ϕ at symmetric points; then Eq. (A-4) can be written as follows:

$$4\pi\phi(P) = \iint_{S_H} \{(\phi-\phi_i)\frac{\partial}{\partial n_H}(\frac{1}{r}+\frac{1}{r'}) - (\frac{1}{r}+\frac{1}{r'})\frac{\partial}{\partial n_H}(\phi-\phi_i)\}\,dS$$

$$- \iint_{S_F} \frac{1}{r}\frac{\partial}{\partial n}(\phi-\bar{\phi})\,dS - \iint_{S_o}\{\phi\frac{\partial}{\partial x'}(\frac{1}{r}+\frac{1}{r'}) - (\frac{1}{r}+\frac{1}{r'})\frac{\partial\phi}{\partial x'}\}\,dS. \qquad \text{(A-5)}$$

Eq. (A-5) can be expressed in terms of source singularities; putting $\phi = \phi_i$, $\partial/\partial n_H\,(\phi-\phi_i) \equiv \sigma_H$ and $\partial/\partial n\,(\phi-\bar{\phi}) \equiv \sigma_F$, we obtain Eq. (1).

Table 1 Principal Paticulars

	M-21	Wigley
L(m)	2.001	3.000
B(m)	0.2368	0.300
d(m)	0.1724	0.1875
$\nabla(m^3)$	0.0347	0.075
$S(m^2)$	0.6686	1.329

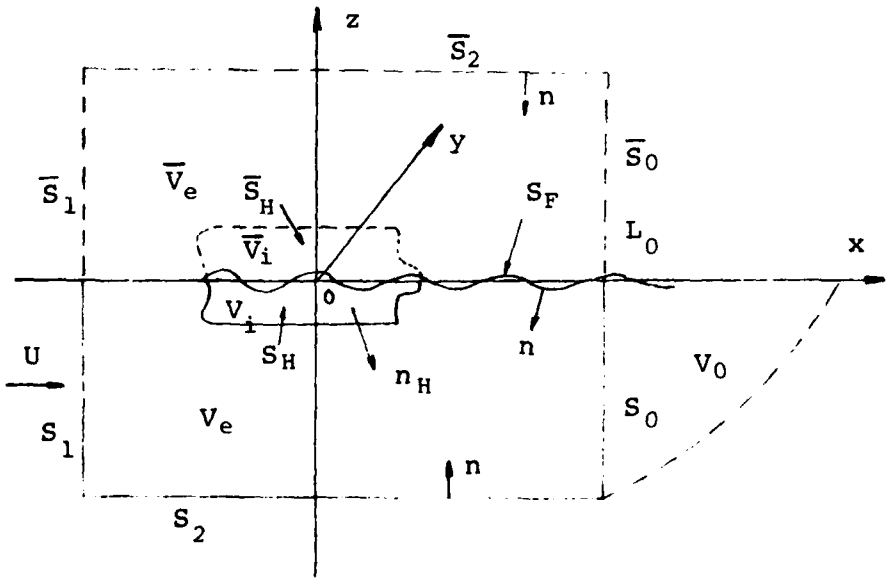

Fig. 1 Coordinate System and Definition

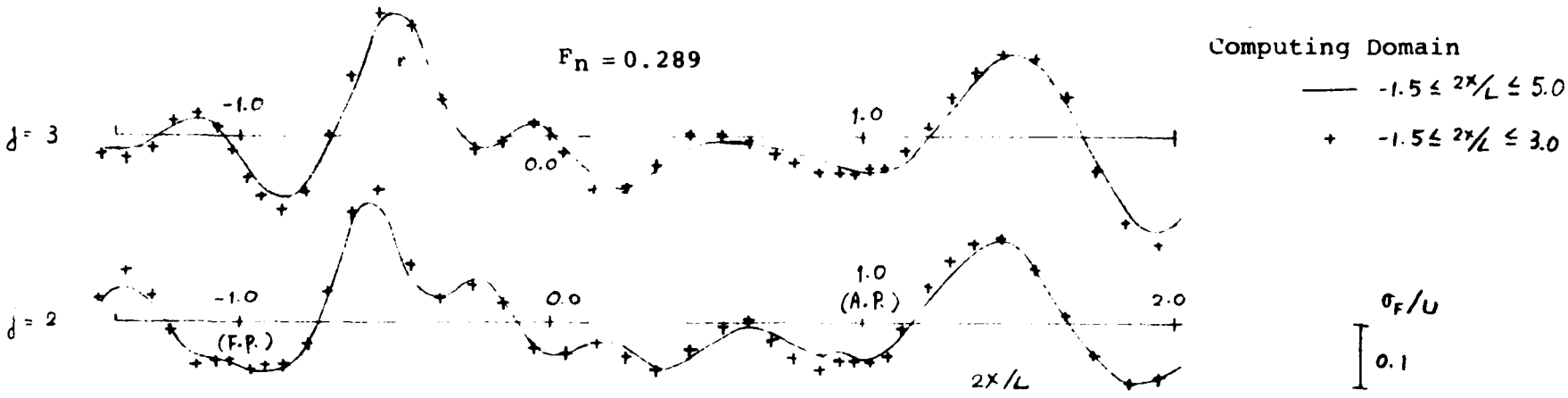

Fig. 3 Source Distribution on Free Surface (M-21)

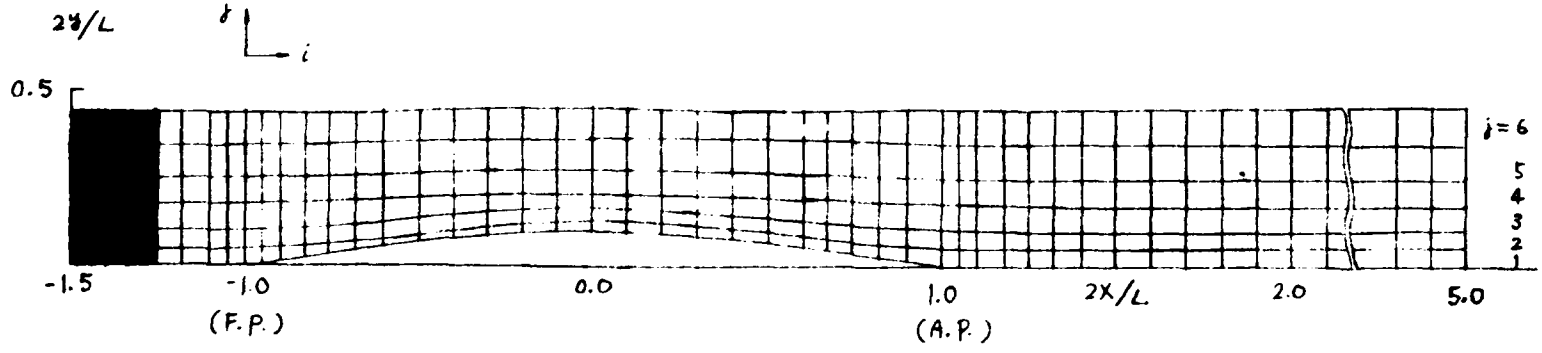

Fig. 2 Discretization of Free Surface (M-21)

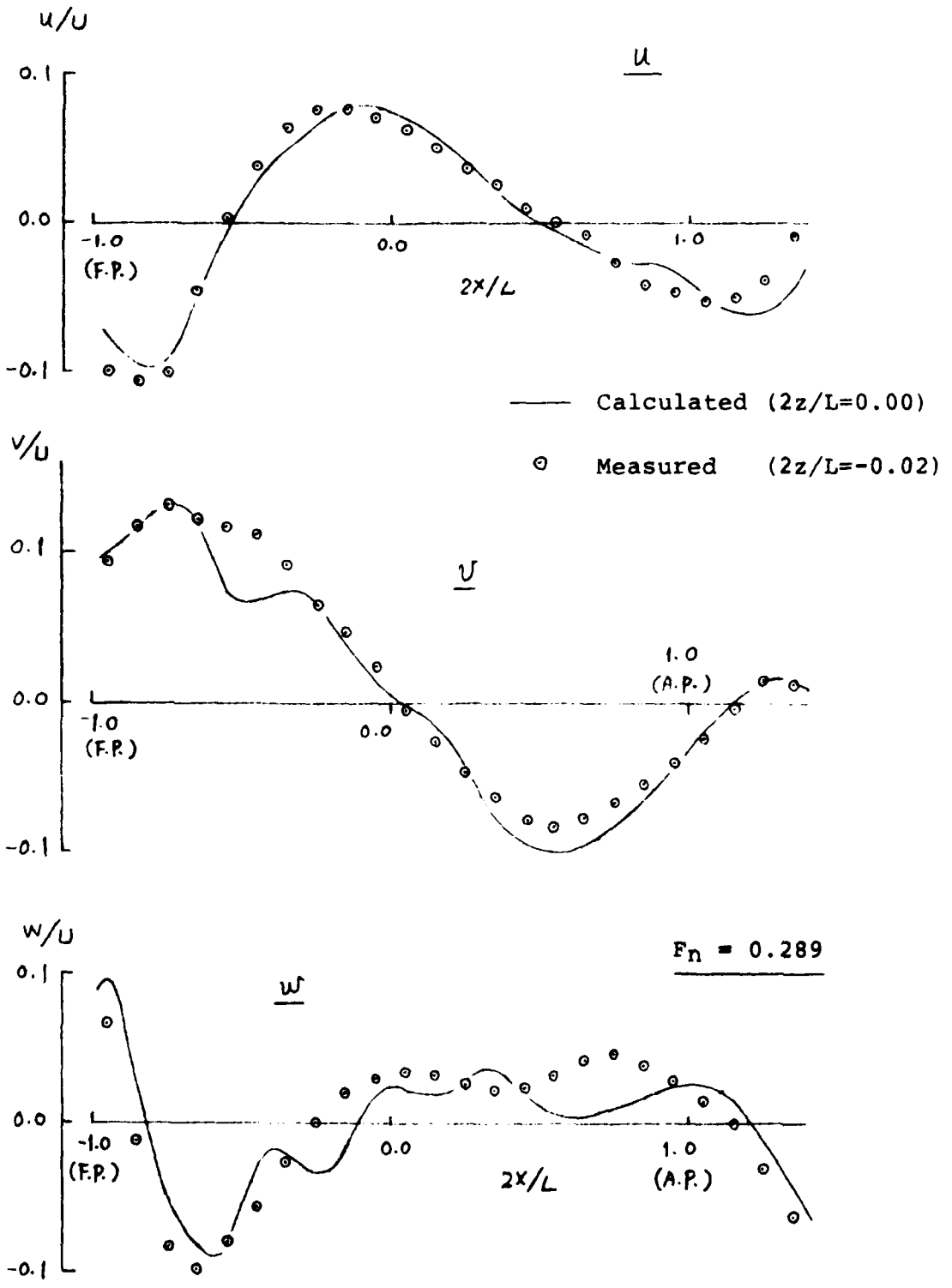

Fig.4a Velocity Distribution of M-21 (z=0.00)

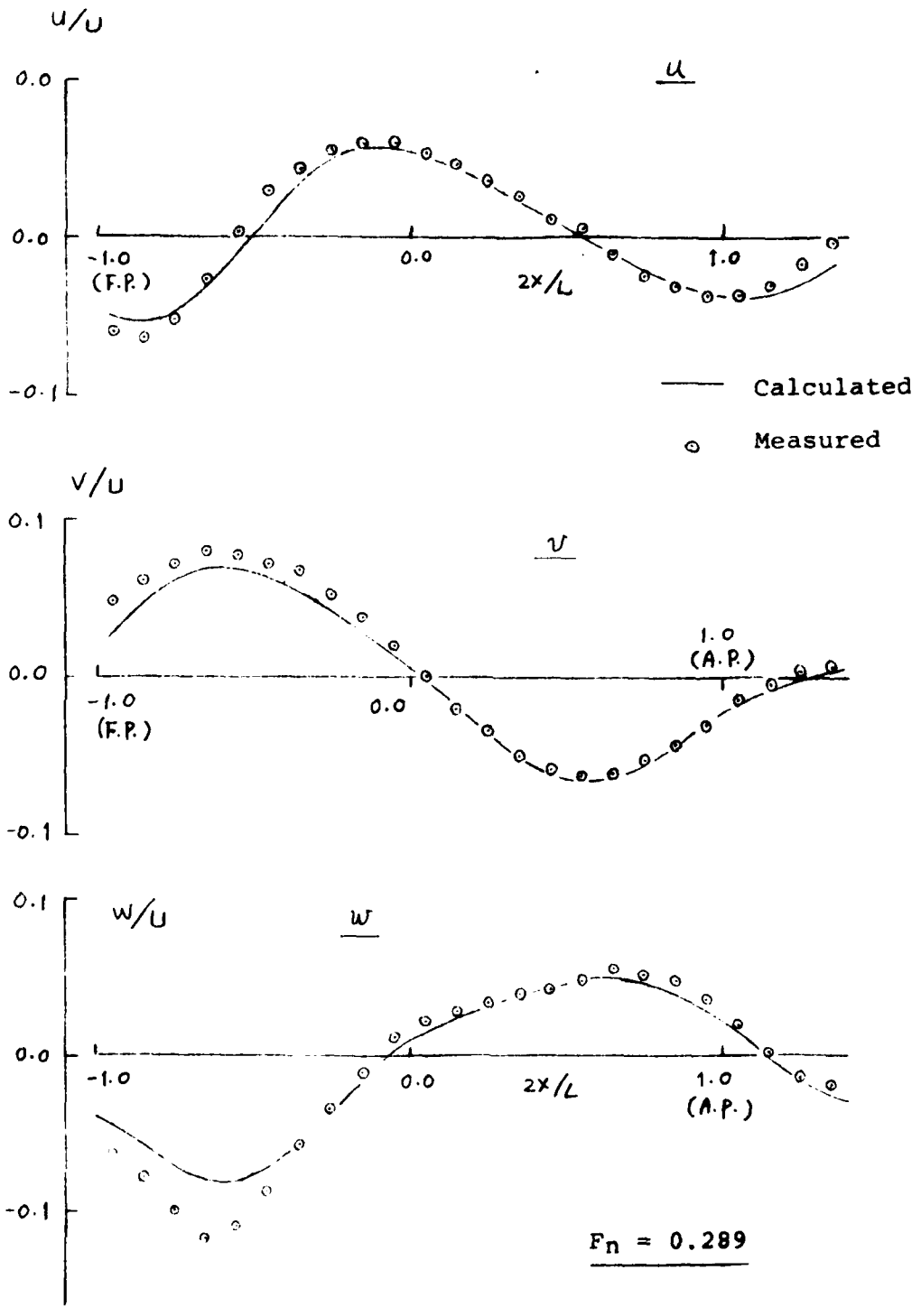

Fig. 4b Velocity Distribution of M-21 (2z/L=-0.10)

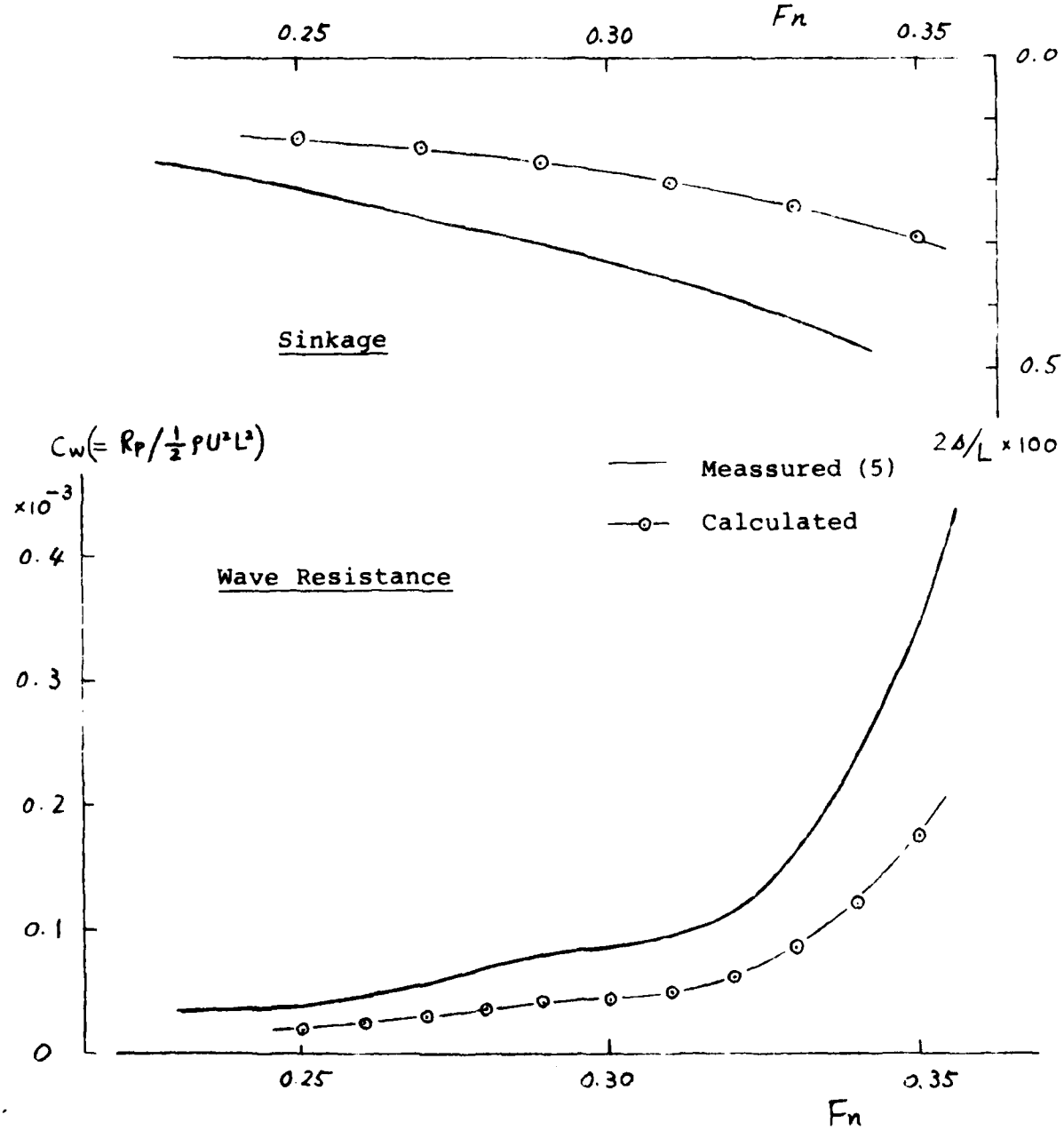

Fig. 5 Wave Resistance and Sinkage of M-21

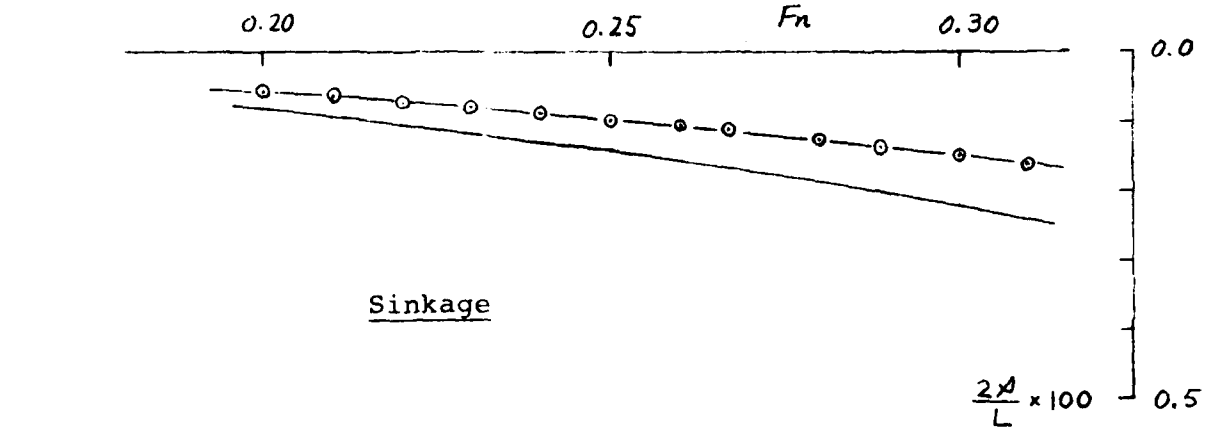

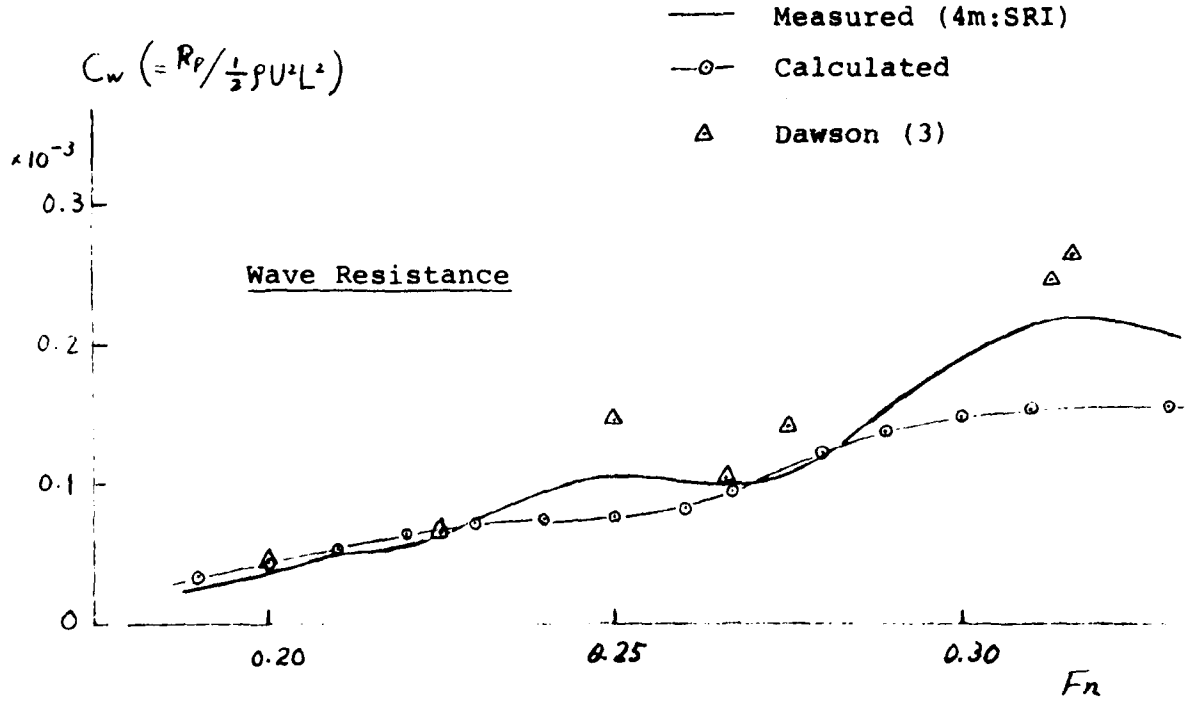

Fig. 6 Wave Resistance and Sinkage of Wigley Model

B. Prediction of 2-D Near-Wake Flow by Making Use of Time-Dependent Vorticity Transport Equation

1. Introduction

This study is an extension of previous work [1] [2] where the flow over a ship stern is predicted by making use of the vorticity transport equation.

In the first paper [1], an approximation is made for the vorticity equation which is basically the same as the first-order boundary-layer approximation. In the second paper [2], several approximations are invoked to predict a significantly separated flow which are then matched with each other. The full equation is applied to a restricted region where a recirculating flow is significant.

In both papers, the boundary-layer equation is applied up to the position where the flow is free from separation, beyond which it is replaced by the vorticity equation. The boundary-layer calculation provides initial or boundary values for the vorticity equation. The total velocity field in the wake is given by a sum of the potential velocity and the induced velocity of vorticity.

An important difference from previous work is that, in the present work, the vorticity equation is used without any simplifications. This means that the governing equation for the wake is completely elliptic. The process of vorticity transportation is solved by the time-marching method. The k-ε model is invoked for the turbulence closure in the present scheme.

Though the vorticity transport equation is exactly identical with the Navier-Stokes equation, it has several advantages over the N-S equation when it is applied to the prediction of near-wake flows of shiplike bodies. First, the velocity field can be obtained by a simple sum of the potential velocity and the velocity induced by vorticity. This removes the troublesome treatments of their interactions, for it is not necessary to distinguish the viscous region from the inviscid. Another desirable feature is that the unknown pressure term is eliminated.

The most important advantage is that the computing domain of the vorticity equation is confined to a nonzero vorticity region. It is more definite and narrower than that of the case where the N-S equation is used.

The boundary values on the downstream and the lateral terminating surfaces are definitely explicit and zero. These advantages make the numerical calculation much simpler.

The only, but important, difficulty is that of providing the boundary values for vorticity on solid bodies. In the present paper, this is treated by a source distribution and a vortex sheet over the body.

Near wakes of a flat plate and two elliptic cylinders are calculated.

2. Basic equations

Restricting ourselves to 2-D cases, we use Cartesian co-ordinates which are attached to the body, as shown in Fig. 1. By the curl operation on the Reynolds equation, we obtain

$$\frac{\partial \omega}{\partial t} = -\{\frac{\partial (u\omega)}{\partial x} + \frac{\partial (v\omega)}{\partial y}\} + (\frac{\partial^2}{\partial x^2} - \frac{\partial^2}{\partial y^2})\{\nu_e(\frac{\partial v}{\partial x} + \frac{\partial u}{\partial y})\} + 2\frac{\partial^2}{\partial x \partial y}\{\nu_e(\frac{\partial v}{\partial y} - \frac{\partial u}{\partial x})\}, \tag{1}$$

where t is the time, u,v are velocity components in x- , y-directions, ω the vorticity with axis normal to the x-y plane, defined by

$$\omega = \frac{\partial v}{\partial x} - \frac{\partial u}{\partial y} \tag{2}$$

and satisfying

$$\frac{\partial \omega}{\partial x} + \frac{\partial \omega}{\partial y} = 0. \tag{3}$$

ν_e is the equivalent eddy kinematic-viscosity coefficient, related to the Reynolds stress by

$$\nu_e = \nu + \nu_t, \tag{4}$$

$$-\overline{u'v'} = \nu_t(\frac{\partial v}{\partial x} + \frac{\partial u}{\partial y}), \tag{5}$$

where ν is the kinematic viscosity, and u',v' are turbulence components of u and v.

The k-ε equations used for the turbulence closure are

$$\frac{\partial k}{\partial t} = -\left\{\frac{\partial (uk)}{\partial x} + \frac{\partial (vk)}{\partial y}\right\} + \frac{\partial}{\partial x}\left(\frac{\nu_e}{\sigma_k}\frac{\partial k}{\partial x}\right) + \frac{\partial}{\partial y}\left(\frac{\nu_e}{\sigma_k}\frac{\partial k}{\partial y}\right) + G'_e - \varepsilon, \tag{6}$$

$$\frac{\partial \varepsilon}{\partial t} = -\left\{\frac{\partial (u\varepsilon)}{\partial x} + \frac{\partial (v\varepsilon)}{\partial y}\right\} + \frac{\partial}{\partial x}\left(\frac{\nu_e}{\sigma_\varepsilon}\frac{\partial \varepsilon}{\partial x}\right) + \frac{\partial}{\partial y}\left(\frac{\nu_e}{\sigma_\varepsilon}\frac{\partial \varepsilon}{\partial y}\right) + C_1 G'_e \frac{\varepsilon}{k} - C_2 \frac{\varepsilon^2}{k}, \tag{7}$$

where

$$G' = \nu_e\left[2\left\{\left(\frac{\partial u}{\partial x}\right)^2 + \left(\frac{\partial v}{\partial y}\right)^2\right\} + \left(\frac{\partial v}{\partial x} + \frac{\partial u}{\partial y}\right)\right]. \tag{8}$$

The five model constants are assigned the following values:

$$C_D = 0.09,\ C_1 = 1.44,\ C_2 = 1.92,\ \sigma_k = 1.00,\ \sigma_\varepsilon = 1.23.$$

Once the vorticity field is determined, the velocity at P(x,y) is given by

$$\begin{Bmatrix} u(x,y) \\ v(x.y) \end{Bmatrix} = -\frac{1}{2\pi}\iint_{\forall} \frac{\omega(x',y')}{(x-x')^2 + (y-y')^2}\begin{Bmatrix} (y-y') \\ -(x-x') \end{Bmatrix} dx'dy' + \begin{Bmatrix} u_o(x,y) \\ v_o(x,y) \end{Bmatrix} \tag{9}$$

where $\forall$ denotes the nonzero vorticity region. The derivation is given in the Appendix. The first term is the velocity induced by the vorticity. Although the solution of Eq. (1) and the integration in Eq. (9) are definitely confined to $\forall$, the induced velocity influences the flow beyond $\forall$. This is the way the viscid and inviscid interaction is taken into account in the present method.

The second term on the r.h.s. of Eq. (9) is the potential components given by

$$u_o = \frac{\partial \phi}{\partial x} + u_1, \qquad v_o = \frac{\partial \phi}{\partial y} + v_1, \tag{10}$$

where ϕ is the total velocity potential.

u_1 and v_1 are the velocity components due to the image vorticity which can be determined in order for u and v to satisfy the hull surface condition; i.e., u = 0, v = 0 on the hull. Wu and Thompson [3] criticized the inclusion of these terms and they used another expression which does not contain them. It is true that their expression is simpler, but it is valid only when the vorticity distribution is obtained such that the velocity satisfies the nonslip condition. As mentioned later, however, this is not possible when Eqs. (1) and (9) are solved iteratively. On the contrary, u_1 and v_1 can be easily determined, as is shown in the Appendix, by making use of a source and vortex distribution. If a constant distribution is assumed along a short segment $\overline{AB}$, u_1 and v_1 at P are given by

$$\begin{aligned} u_1 &= -\sigma_1 \log \frac{\overline{BP}}{\overline{AP}} - \frac{\gamma_1}{2\pi} < APB, \\ v_1 &= \sigma_1 < APB - \frac{\gamma_1}{2\pi} \log \frac{\overline{BP}}{\overline{AP}}, \end{aligned} \tag{11}$$

where σ_1 and γ_1 are the strengths of the source and vortex sheet respectively which are determined so as to satisfy the hull-surface condition.

3. Computing scheme

We assume that, initially, a vorticity region over the surface of a body is generated by a sudden motion of the body to a constant speed of U. The flow is then irrotational except in the vorticity layer (boundary layer). Subsequently, a wake--nonzero vorticity region--is formed in the vicinity of the stern by the diffusion and convection of vorticity. Thus, finally, a steady (or quasi-steady) wake is formed.

This idealization provides the following computing scheme for this initial and boundary-value problem. First, we carry out the boundary-layer calculation up to points beyond which the flow is affected by separation. Then we solve Eqs. (4)-(8) and Eq. (1) with given boundary values and a prescribed velocity field. Next, the velocity field is determined by Eqs. (9) and (10). The latter two calculations are repeated successively in the following order until the solution converges;

$$1.\quad \{\varepsilon^k\}^{(n+1)} = \{\varepsilon^k\}^{(n)} + \Delta t^{(n)} f_{k,\varepsilon}(q^{(n)}, k^{(n)}, \varepsilon^{(n)}, \nu_e^{(n)}), \tag{12}$$

$$2.\quad \omega^{(n+1)} = \omega^{(n)} + \Delta t^{(n)} f_{\omega}(\omega^{(n)}, \mathbf{q}^{(n)}, \nu_e^{(n+1)}), \tag{13}$$

$$3.\quad \mathbf{q}^{(n+1)} = f_q(\omega^{(n+1)}, \sigma_1^{(n+1)}, \gamma_1^{(n+1)}) + \nabla\phi, \tag{14}$$

where the superscript (n) refers to values at $t = t^{(n)}$. If all the values at $t = t^{(n)}$ are known and necessary boundary values are given, Eqs. (12) and (13) can be solved in the computing domain $\forall^{(n+1)}$. The computing domain expands as time elapses in order to include the region of nonzero vorticity with zero value on the boundary.

Initial values, at $t = 0$, are tabulated in Table 1. B_{BL}, B_H, B_X, B_Y, B_{SYM} are boundaries surrounding the computing domain $\forall$ (see Fig. 1). Suffix BL refers to values obtained by the boundary-layer calculation. Nonzero initial values for k and ε are used partially in $\forall(2x/L < 1.2)$. This is because the vorticity on B_H does not diffuse so much if k and ε are zero everywhere in $\forall$.

The boundary values are shown in Table 2.

As mentioned already, we cannot have any specified values for vorticity on the solid body. This is an unavoidable difficulty of the present method where the vorticity equation is used. In our scheme we supply this with

$$\omega_0^{(n+1)} = q_t^{(n)}/\Delta, \tag{15}$$

where Δ is a short distance normal to the hull surface and q_t is the resultant velocity. Eq. (15) is obtained by making use of the nonslip condition, but it does not always guarantee the satisfaction of the nonslip condition at the (n+1)-th step. σ_1 and γ_1 are determined for the velocity at the (n+1)-th step to satisfy the hull-surface condition. At the first time step, n=0, the potential velocity is used; $q_t^{(0)} = |\nabla\phi|$.

As mentioned above, the computing domain must be expanded indefinitely. In reality, however, it must be truncated. After B_X has arrived at some position beyond which the computing domain is not extended further, $\partial^2\omega/\partial x^2 = 0$ is imposed as a boundary condition on B_X.

Δt, in Eqs. (12) and (13), is the time step. In the present scheme, according to Von-Neumann's analysis [4], it is taken as

$$\Delta t = \text{Min}\left\{ \frac{1}{2\nu_e\left(\frac{1}{\Delta x^2} + \frac{1}{\Delta y^2}\right) + \frac{|u|}{\Delta x} + \frac{|v|}{\Delta y}} \right\}, \qquad (16)$$

where Min { } refers to the minimum of the arguments defined in the whole computing domain. Δx and Δy are grid sizes.

$f_{k,\varepsilon}$ and f_ω are finite-difference expressions of the r.h.s. of Eqs. (1), (6) and (7). The second upwind-differencing method [4] is used for the first (convection) terms on the r.h.s. of Eqs. (1), (6) and (7). On the other hand, central differences are used for the diffusion terms.

Boundary-layer calculations are carried out by the integral method, with Head's entrainment formula used as an auxiliary equation.

4. Numerical results and discussions

4.1 Flat plate

The main purpose of the calculation for a flat plate is to examine the present scheme and numerical techniques. All the computing conditions were adjusted to those of the experiment of Chevray et al [5]. The overall length L is 2.4m and the origin is shifted to the leading edge for this case. The Reynolds number based on L is 6.545×10^5.

Results are shown in Figs. 2-5. The positions where comparisons are made with the measurements do not exactly correspond; the computed results at x/L = 1.025, 1.080, 1.200, 1.600 are compared with experimental data at x/L = 1.020, 1.083, 1.208 and 1.625 respectively (only the former numbers are used later on). The results are those at t = 0.917 L/U, when the computing domain has expanded to x = 1.72L and y = 0.032L.

Good agreement with experiment was obtained everywhere except far downstream at x/L = 1.60. The numerical computations were completely stable.

Needless to say, because the vorticity beyond the terminating surface (x = 1.72L) is not included, the poor agreement far downstream (x= 1.60L) can be partially attributed to this exclusion. Furthermore, a possible invalidity of the use of the k-ε model far downstream may be mentioned. Recently, through

precise comparisons with experimental data, Ramaprian et al [6] and Patel et al [7] have pointed out that the basic k-ε model does not lead to a theoretically expected asymptotic flow in a far wake due to a different behavior of the intermittency.

As far as the near wake flow is concerned, however, we can conclude that the present scheme works well and satisfactory predictions can be obtained.

4.2 Elliptic cylinder

Calculations were performed for two elliptic cylinders designated EM-125 and EM-200, having ratios b of the major and minor axes of 0.125 and 0.200 respectively [8]. The velocity measurements were carried out by making use of a five-hole pitot tube. An eight-hole pipe, which has eight holes along the circumference of a circular pipe, was also used to follow reverse flows. The referred Reynolds numbers of EM-125 and EM-200 are 1.68×10^6 respectively.

The potential velocity components are given by

$$\frac{\partial \phi}{\partial x} = U + \frac{1 + b}{2(1 + b^2)} \frac{\cosh 2\xi - \cosh 2\eta - b \sinh 2\xi}{\cosh^2 \xi - \cos^2 \eta} U,$$

$$\frac{\partial \phi}{\partial y} = - \frac{b(1 + b)}{2(1 + b^2)} \frac{\sin 2\eta}{\cosh^2 \xi - \cos^2 \eta} U, \tag{17}$$

where

$$x + iy = \sqrt{1 + b^2} \cosh (\xi - i\eta). \tag{18}$$

The boundary-layer calculations were carried out by making use of the momentum-thickness equation and the entrainment equation. The calculated momentum thickness, θ, shape factor, H, boundary-layer thickness, δ, and shearing stress, τ, are shown in Fig. 6. B_{BL}, where the governing equation is changed into the vorticity equation, is chosen at $2x/L = 0.8$ in order to have reliable values for initial and boundary values.

In Figs. 7-9, calculated results of EM-125 are shown.

Fig. 7 shows the velocity and the vorticity distributions at $2x/L = 0.905$ and 1.10. Calculated results, shown at every 0.1 L/U time step, seem to converge. Agreement with the measurements is not so good at $2x/L = 1.10$ as that at $2x/L = 0.905$.

In our scheme, we imposed the symmetry condition on $y = 0(B_{SYM})$. We suspect that this boundary condition may be the cause of this disagreement. As is seen in Fig. 9, a vortex behind the body is predicted. This is growing steadily and symmetrically. Experimentally, however, it is observed that vortices are unsteady and moving across the symmetry plane. At $2x/L = 0.905$, flows may not be affected so much by the symmetry condition. It may be necessary, though the computing time and the storage may increase, to remove the symmetry condition and to introduce a slight disturbance to obtain a more realistic flow.

Fig. 8 shows the turbulence quantities. Undesirable changes, observed in the results at $2x/L = 0.905$ around $2y/L = 0.06$, are after-effects of Cebeci-Smith's model which is invoked to determine the boundary values of k and ε on B_{BL}.

Fig. 9 shows the flow patterns at three time steps. Vectors show the velocity and the flow direction. It is predicted that separation is occurring around $2x/L = 0.975$.

Calculated results of EM-200 are shown in Figs. 10 and 11. Fig. 10 shows the computed results at $2x/L = 0.95$ and 1.10. Here the calculations were carried out up to $t = 0.4L/U$. A much longer time than this is needed for the results to converge, especially far downstream. Indeed, there is a possibility that the results may not converge. Although some significant discrepancies from measurements are observed, it can be said that the present method predicts the near wake flow fairly well.

Fig. 11 depicts the development of the wake; the symmetric vortex becomes strong and eventually a significant reverse flow is realized. The separation position is predicted to occur around $2x/L = 0.925$.

These calculations for the elliptic cylinders raise doubts as to whether we can expect a steady or quasi-steady flow in the wake. It appears to be necessary to remove the symmetric flow condition at least.

5. Concluding remarks

We can conclude that the present scheme, where the time-dependent vorticity transport equation is used in its full form together with the boundary-layer equation, is promising. Several modifications in numerical techniques seem to be required; e.g., the prescribed boundary values of the vorticity need to be improved. It can be also said that the k-ε turbulence model is applicable for a near wake prediction.

Though it is not our main purpose to discuss experiments, it is highly necessary to carry out precise velocity measurements in the near wake of blunt bodies which can provide not only averaged quantities but also time-dependent quantities. This would give a much better understanding of separated flows and accelerate development of numerical calculation procedures.

References

1) Hatano, S., Mori, K, Fukushima, M. and Yamazaki, R.; Calculation of Velocity Distributions in Ship Wake, Jour. of Soc. of Naval Arch. of Japan, Vol. 139 (1975).

2) Mori, K. and Doi, Y.; Approximate Prediction of Flow Field around Ship Stern by Asymptotic Expansion Method, Journ. of Soc. of Naval Arch. of Japan, Vol. 144 (1978).

3) Wu, J.C. and Thompson, J.F.; Numerical Solutions of Time-Dependent Incompressible Navier-Stokes Equations Using an Integro-Differential Formulation, Computers and Fluids, Vol. 1 (1973).

4) Roache, P.J.; Computational Fluid Dynamics, hermos publishers, (1976).

5) Chevray, R. and Kovasznay, L.S.G.; Turbulence Measurements in the Wake of a Thin Flat plate; AIAA Journ. Vol. 7 (1969).

6) Ramaprian, B.R., Patel, V.C. and Sastry, M.S.; Turbulent Wake Developement behind Streamlined Bodies, IIHR Report No. 231 (1981).

7) Patel, V.C. and Scheuerer, G.; Calculation of Two-Dimensional Near and Far Wakes, AIAA Journ. Vol. 20, Number 7 (1982).

8) Mori, K.; Calculation of Near Wake Flow and Resistance of Elliptic-Waterplane Ships, Proc. of Thirteenth Symposium on Naval Hydrodynamics, (1980).

Appendix

Let q_v be a velocity component due to a vorticity distribution ω. Because q_v satisfies the continuity equation, it can be expressed in terms of a vector potential E in the form

$$q_v = \nabla \times E, \qquad \nabla . E = 0 \tag{A-1}$$

A curl operation applied to Eq. (A-1) then yields

$$\nabla^2 E = - \omega. \tag{A-3}$$

Thus the vector function E is a solution of the Poisson equation given by Eq. (A-3).

By making use of Green's theorem in the domain exterior to the body, we obtain

$$4\pi E = \iiint_{V} \frac{\omega'}{r} dV' + \iint_{S_B + S_\infty} \left(\frac{1}{r} \frac{\partial E'}{\partial n} - E' \frac{\partial}{\partial n} \frac{1}{r}\right) dS', \tag{A-4}$$

where V is the nonzero vorticity region surrounded by S_B and S_∞ which are a body surface and a closing surface at infinity respectively; n denotes distance along the outward normal to $S_B + S_\infty$, r is the distance between the field point and the integrating point; primes indicate the values at the latter point.

If ω tends to zero at the rate of $1/R^3$, where R is the distance to S_∞, since E vanishes as 1/R, the integration over S_∞ becomes infinitesimally small when R is chosen large enough. Then we have

$$4\pi E = \iiint_{V} \frac{\omega'}{r} dV' + \iint_{S_B} \left(\frac{1}{r} \frac{\partial E'}{\partial n} - E' \frac{\partial}{\partial n} \frac{1}{r}\right) dS'. \tag{A-5}$$

Now we assume another vorticity distribution ω' inside S_B. Similarly to Eq. (A-3) we have

$$\nabla^2 E_1 = - \omega_1. \tag{A-6}$$

By applying Green's theorem to the interior domain of S_B, we get

$$0 = \iiint_B \frac{\omega_1'}{r}\, d\forall' - \iint_{S_B} \left(\frac{1}{r}\frac{\partial E_1'}{\partial n} - E_1 \frac{\partial}{\partial n}\frac{1}{r}\right) dS' \qquad \text{(A-7)}$$

where B denotes the domain interior to S_B.

The addition of Eq. (A-7) to Eq. (A-5) yields

$$4\pi \mathbf{E} = \iiint_{\forall} \frac{\omega'}{r}\, dv' + \iiint_B \frac{\omega_1'}{r}\, d\forall'$$
$$+ \iint_{S_B} \left\{\frac{1}{r}\frac{\partial}{\partial n}(\mathbf{E}' - \mathbf{E}_1') - (\mathbf{E}' - \mathbf{E}'_1)\frac{\partial}{\partial n}\frac{1}{r}\right\} dS'.$$

If we are concerned with only the exterior flow, we may put

$$\mathbf{E}_1 = \mathbf{E} \qquad \gamma_1 = \frac{\partial}{\partial n}(\mathbf{E} - \mathbf{E}_1) \quad \text{on } S_B, \qquad \text{(A-9)}$$

where γ_1 is a circulation distribution whose direction is tangential to S_B. Then Eq. (A-8) is written as

$$4\pi\, \mathbf{E} = \iiint_{\forall} \frac{\omega'}{r}\, d\forall' + \iiint_B \frac{\omega_1'}{r}\, d\forall' + \iint \frac{\gamma_1'}{r}\, dS' \qquad \text{(A-10)}$$

Eq. (A-10) gives a solution of Eq. (A-3). Because it can be easily proved that **E**, given by Eq. (A-10), satisfies Eq. (A-2), the induced velocity is given by

$$4\pi\, \mathbf{q}_v = \iiint_{\forall} \left(\nabla \times \frac{\omega'}{r}\right) d\forall' + \iiint_B \left(\nabla \times \frac{\omega_1'}{r}\right) d\forall' + \iint_{S_B} \left(\nabla \times \frac{\gamma_1'}{r}\right) dS' \qquad \text{(A-11)}$$

Because the second term on r.h.s. of Eq. (A-11) has a potential in $\forall$ (this can be easily proved by taking the curl operation to it), it can be replaced by a source distribution over S_B. Then we have finally

$$4\pi \mathbf{q}_v = \iiint_{\forall} \left(\nabla \times \frac{\omega'}{r}\right) d\forall' - \nabla \iint_{S_B} \frac{\sigma_1'}{r}\, dS' + \iint_{S_B} \left(\nabla \times \frac{\gamma_1'}{r}\right) dS', \qquad \text{(A-12)}$$

where σ_1 and γ_1 are determined so as to satisfy the hull surface condition.

The addition of the velocity component given by $\nabla\phi$ gives the expression of Eq. (9) in the text.

Table 1 Initial Conditions

	V	B_{BL}	B_H
k	k_{BL}, 0	k_{BL}	0
ε	ε_{BL}, 0	ε_{BL}	0
ω	0	ω_{BL}	ω_o
q	$\nabla\phi$	q_{BL}	0

Table 2 Boundary Conditions

	B_{BL}	B_H	B_{SYM}	B_Y	B_X
k	k_{BL}	0	$\partial k/\partial y = 0$	0	0
ε	ε_{BL}	0	$\partial \varepsilon/\partial y = 0$	0	0
ω	ω_{BL}	ω_o	0	0	0, $\partial^2\omega/\partial x^2 = 0$
$q(\sigma_1, \zeta_1)$	—	0	—	—	—

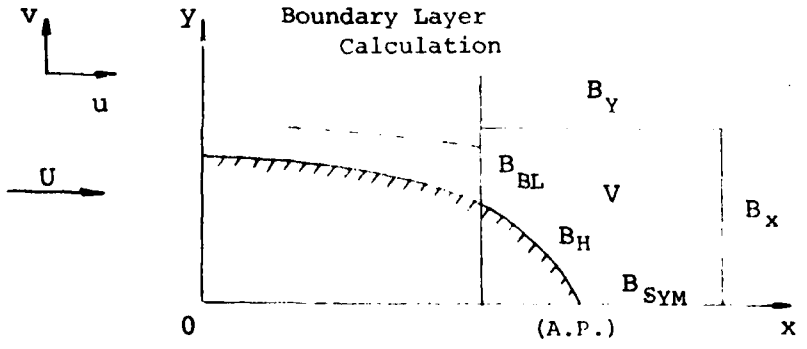

Fig.1 Coordinate System and Definitions

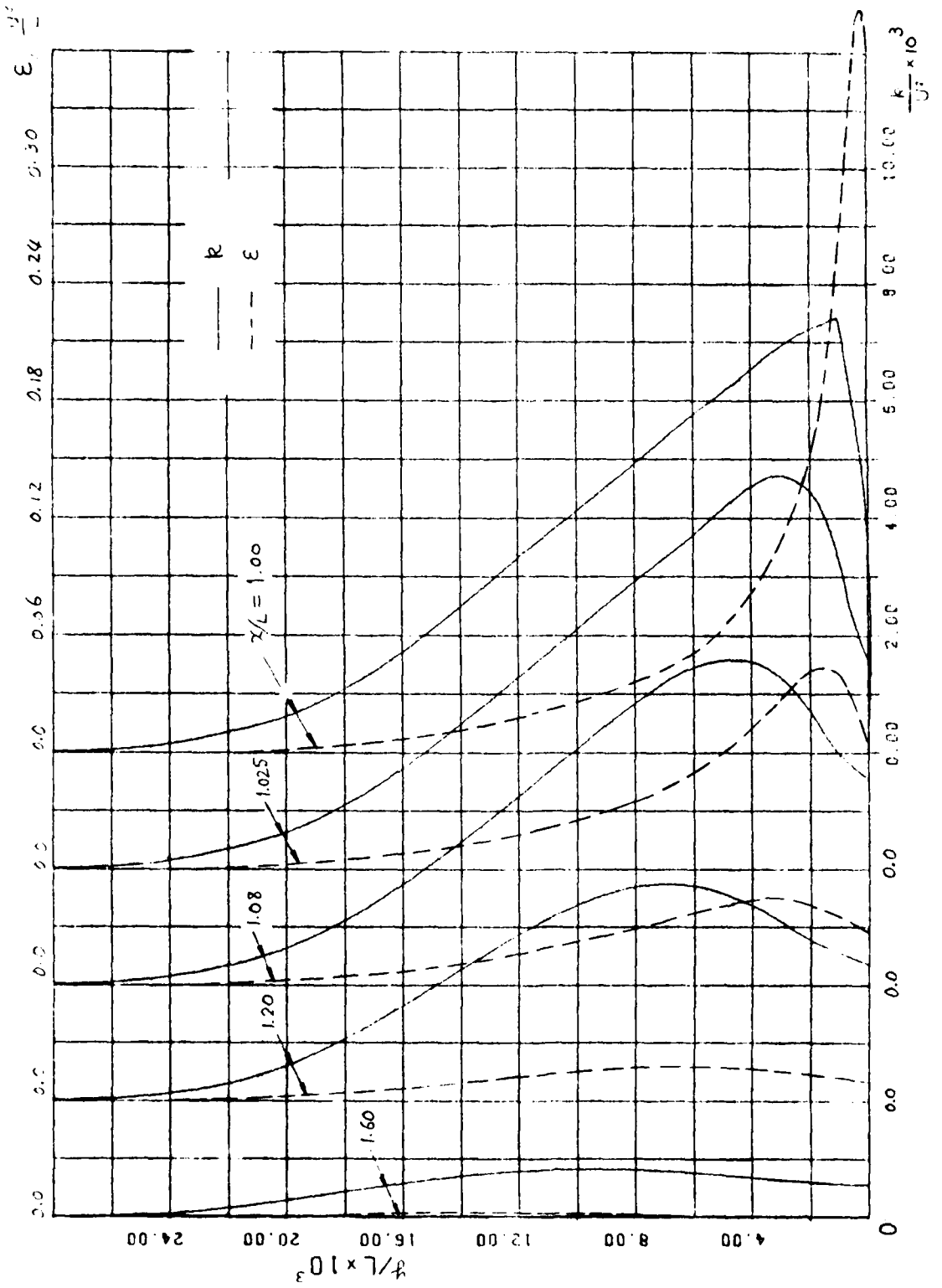

Fig. 2 Calculated k and ε of Flat Plate

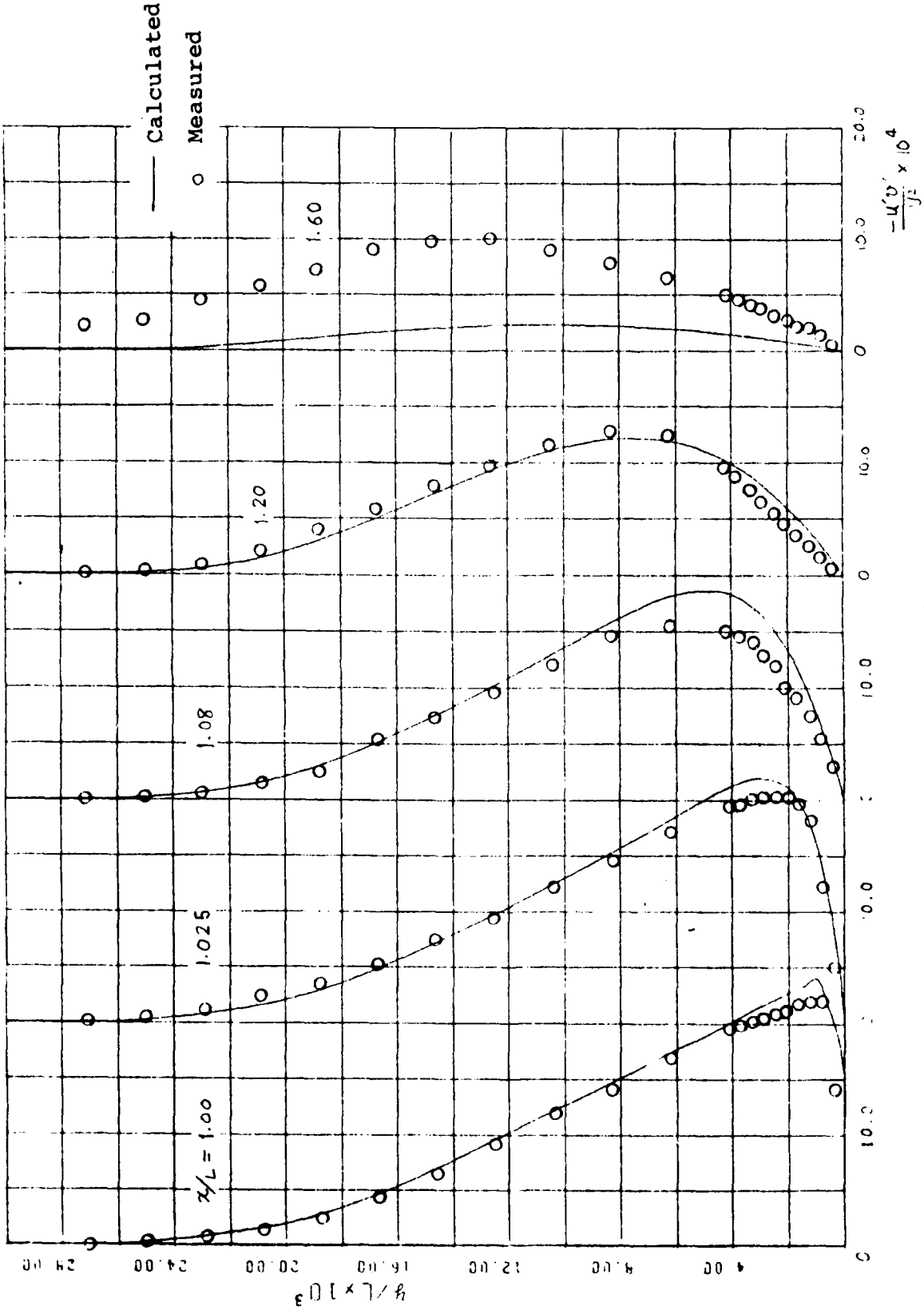

Fig. 3 Reynolds Stress Distribution of Flat Plate

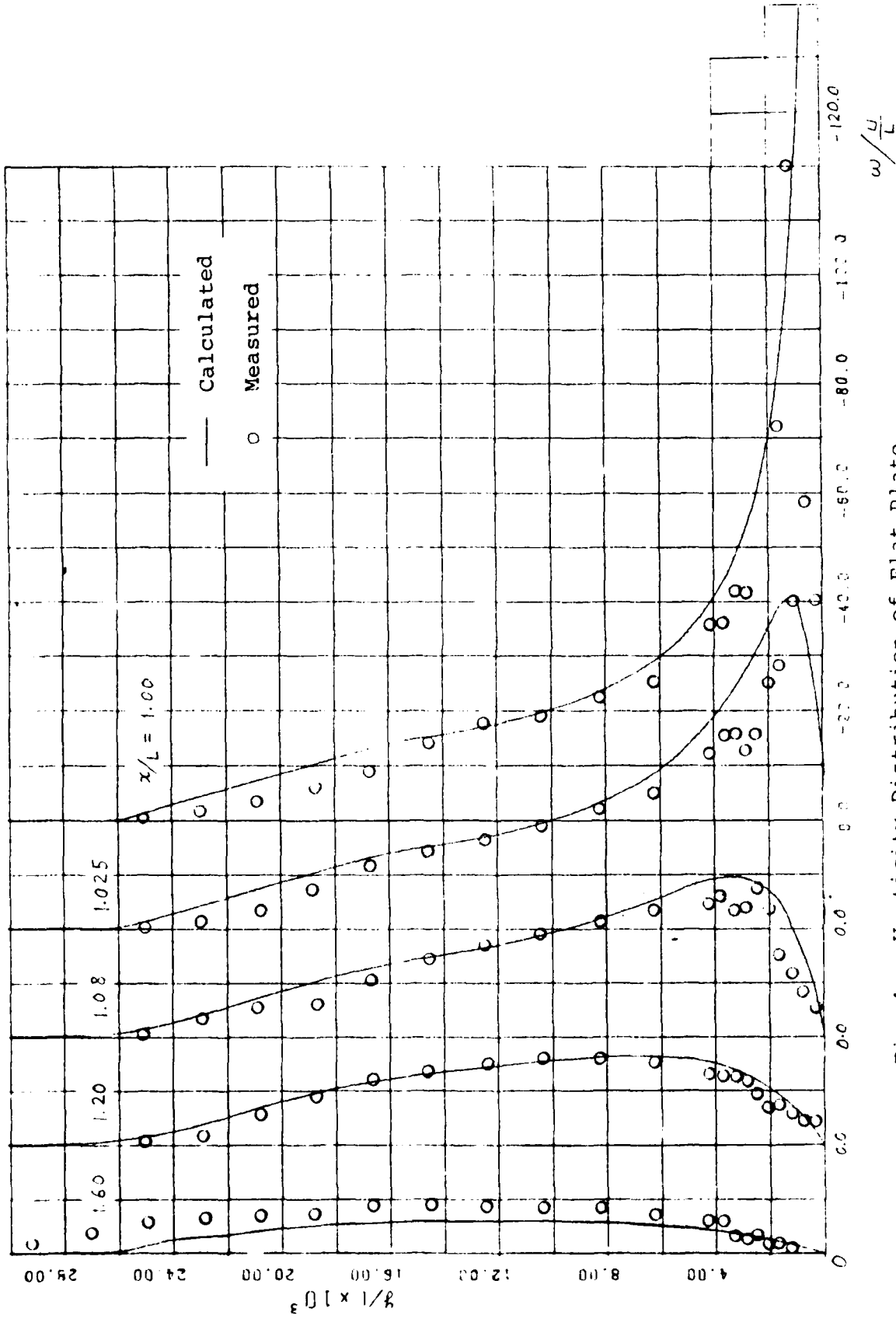

Fig. 4 Vorticity Distribution of Flat Plate

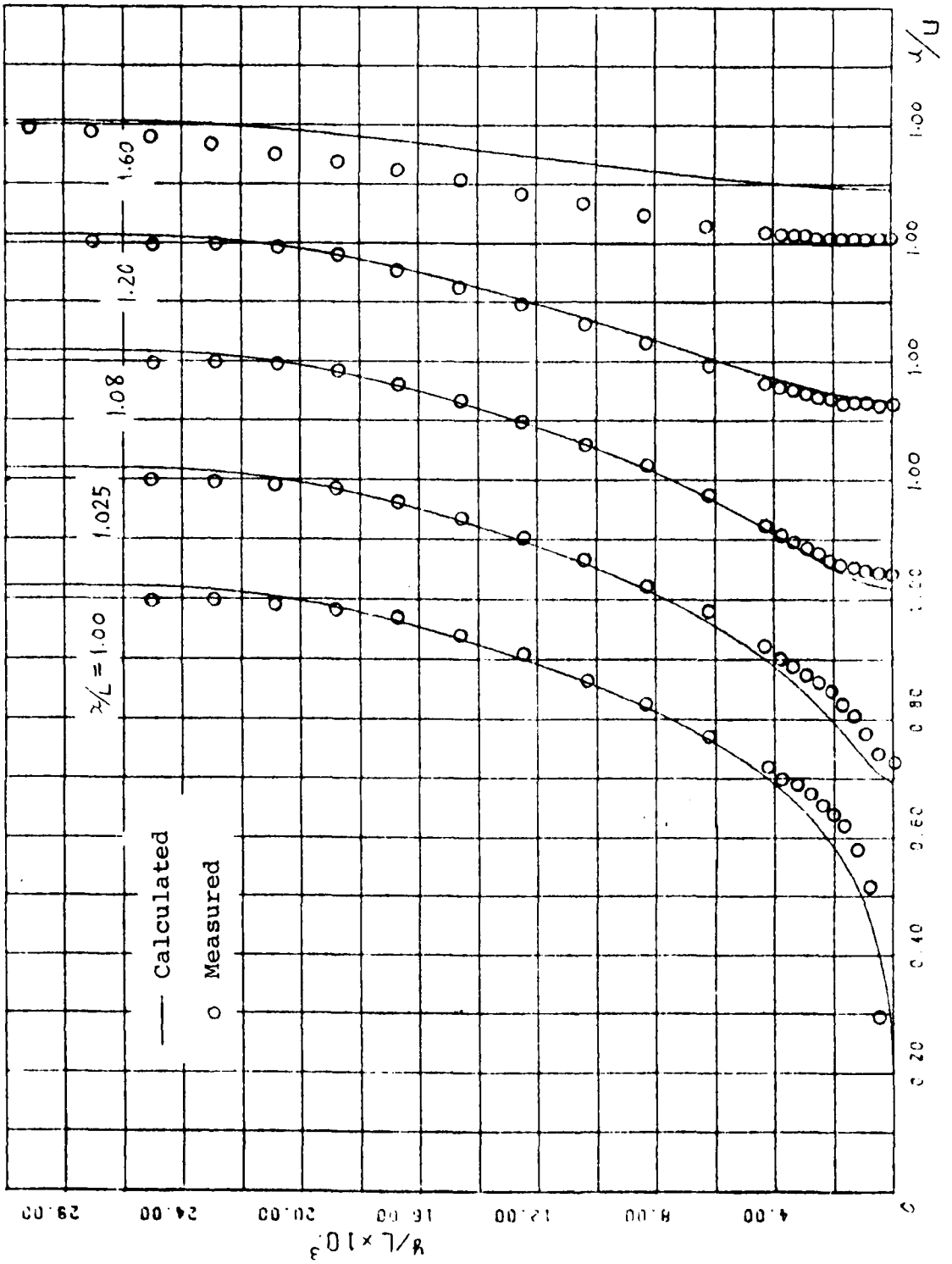

Fig. 5 Velocity Distribution of Flat Plate

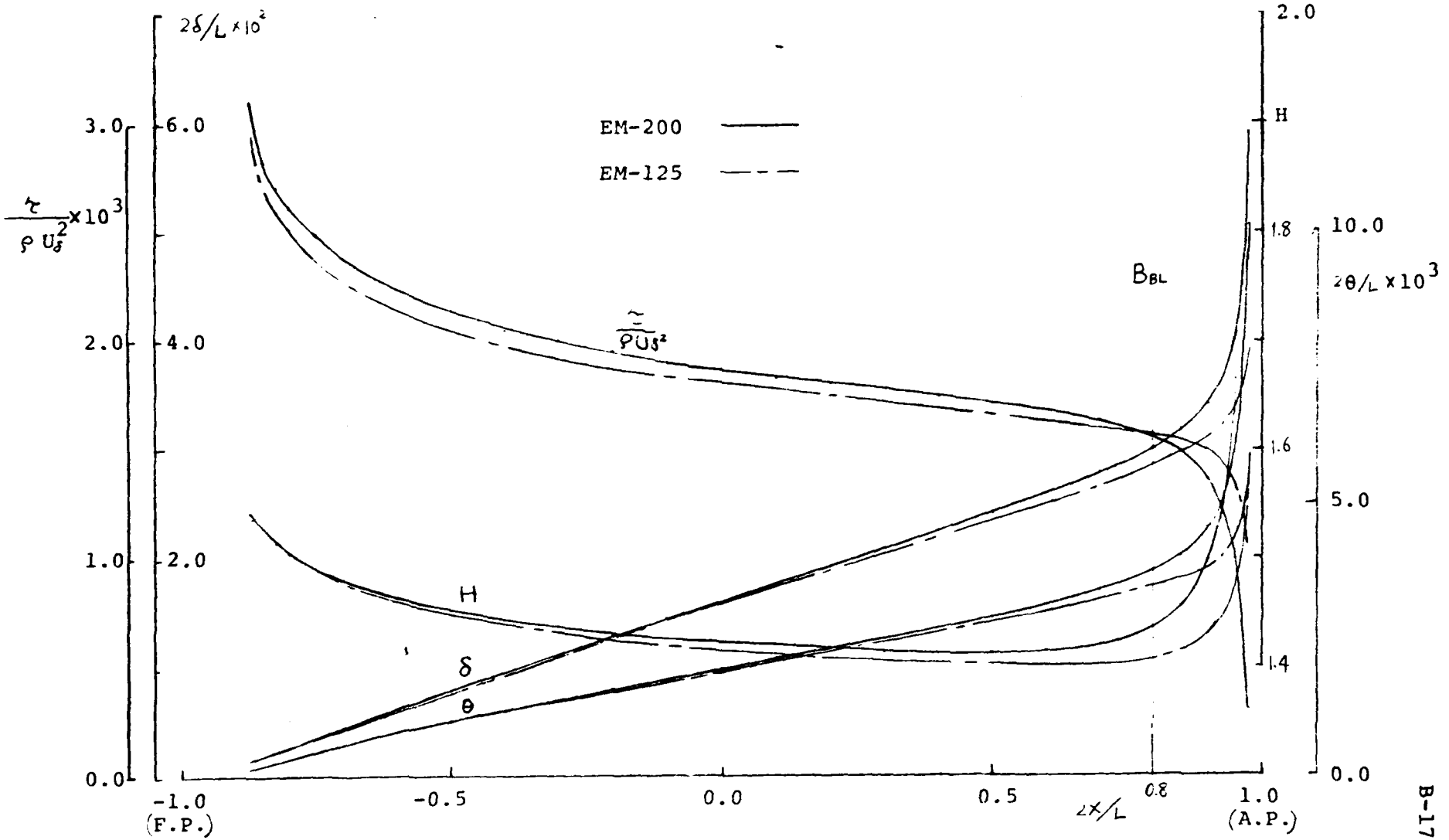

Fig.6 Results of Boundary Layer Calculations (EM-125 & EM-200)

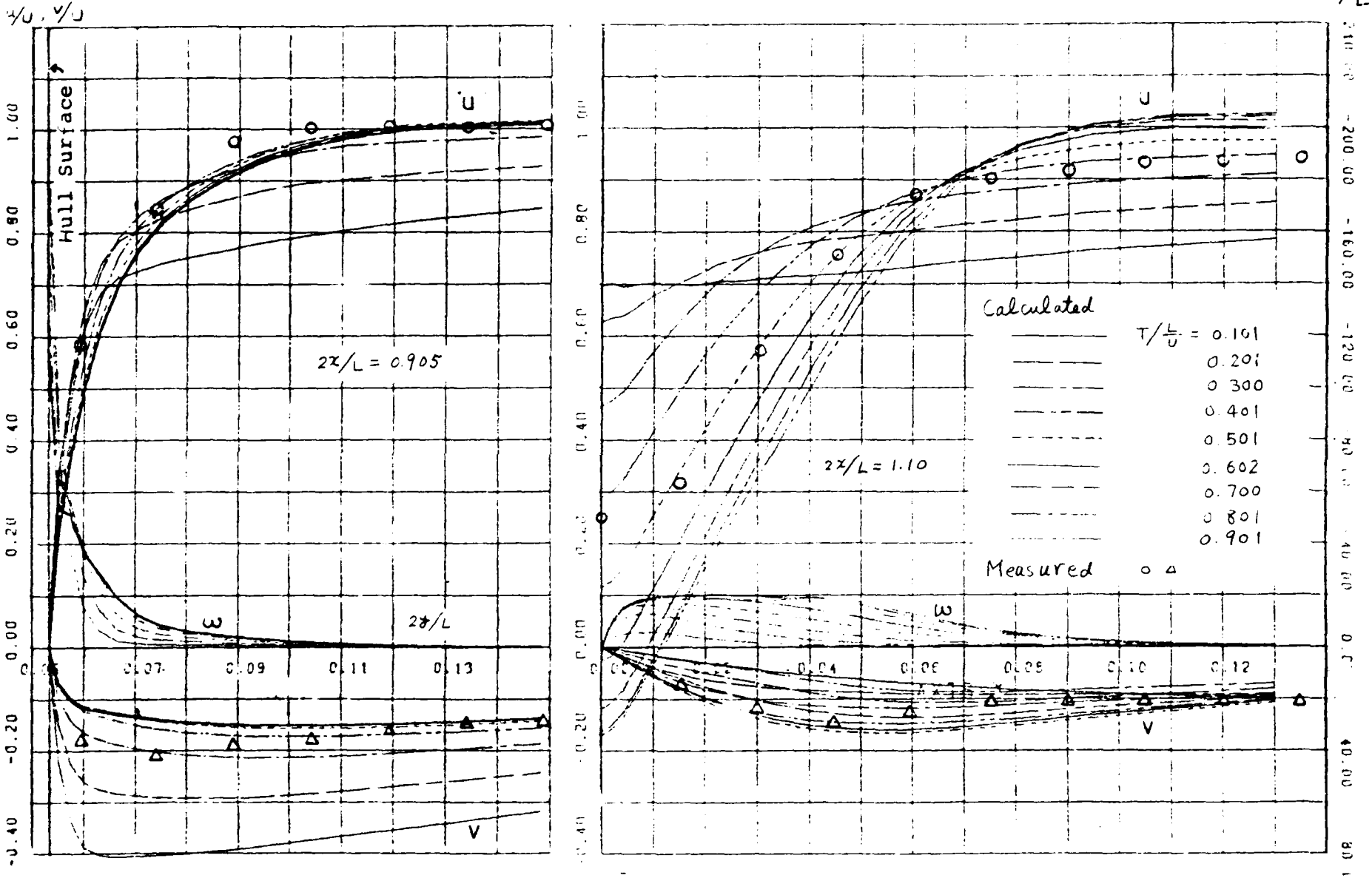

Fig. 7 Comparisons of Velocity Proffiles (EM-125)

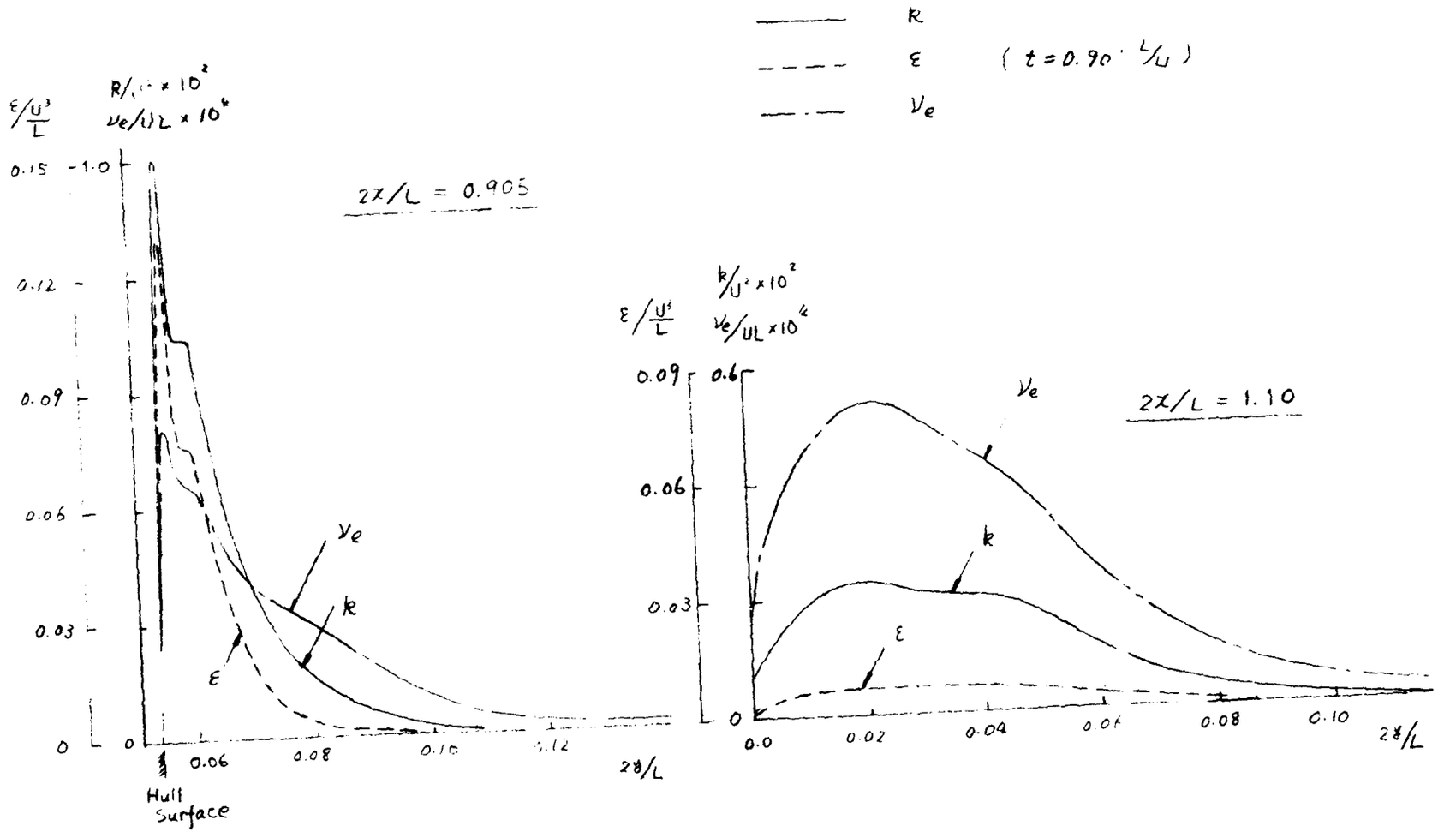

Fig. 8 Calculated Resulta of k, ε and ν_e (EM-125)

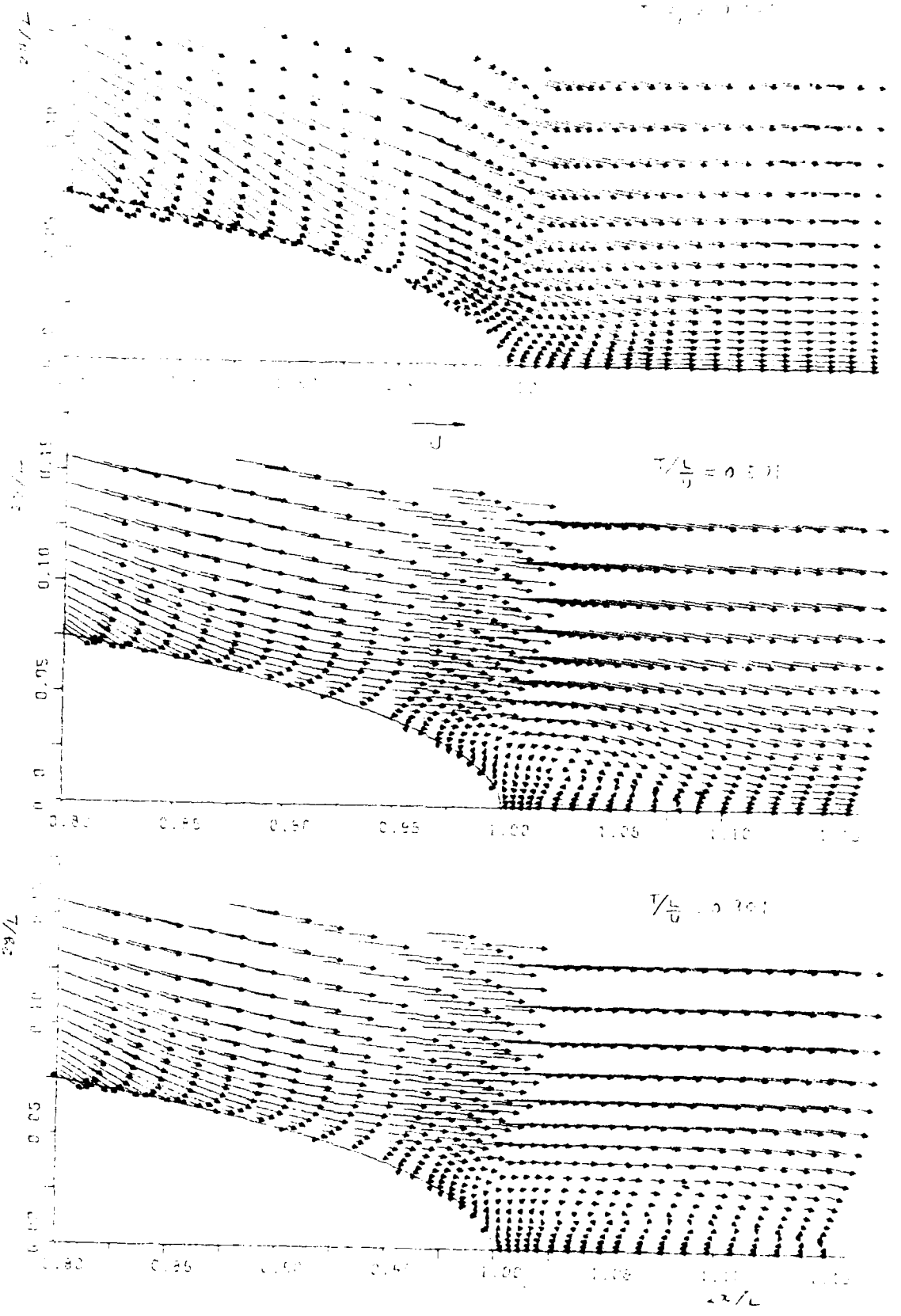

Fig. 9 Calculated Flow Patterns (EM-125)

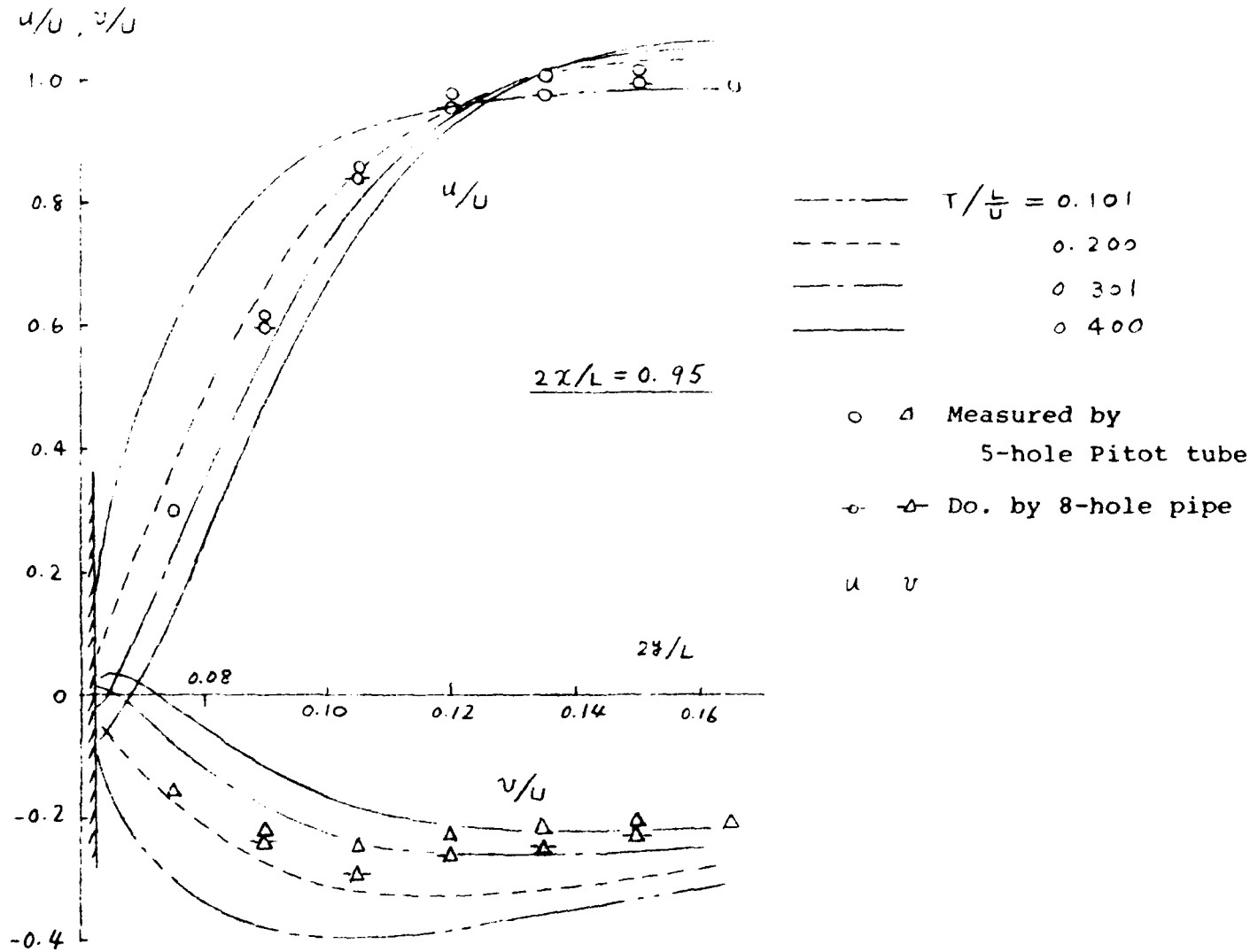

Fig. 10a Comparisons of Velocity Profiles (EM-200)

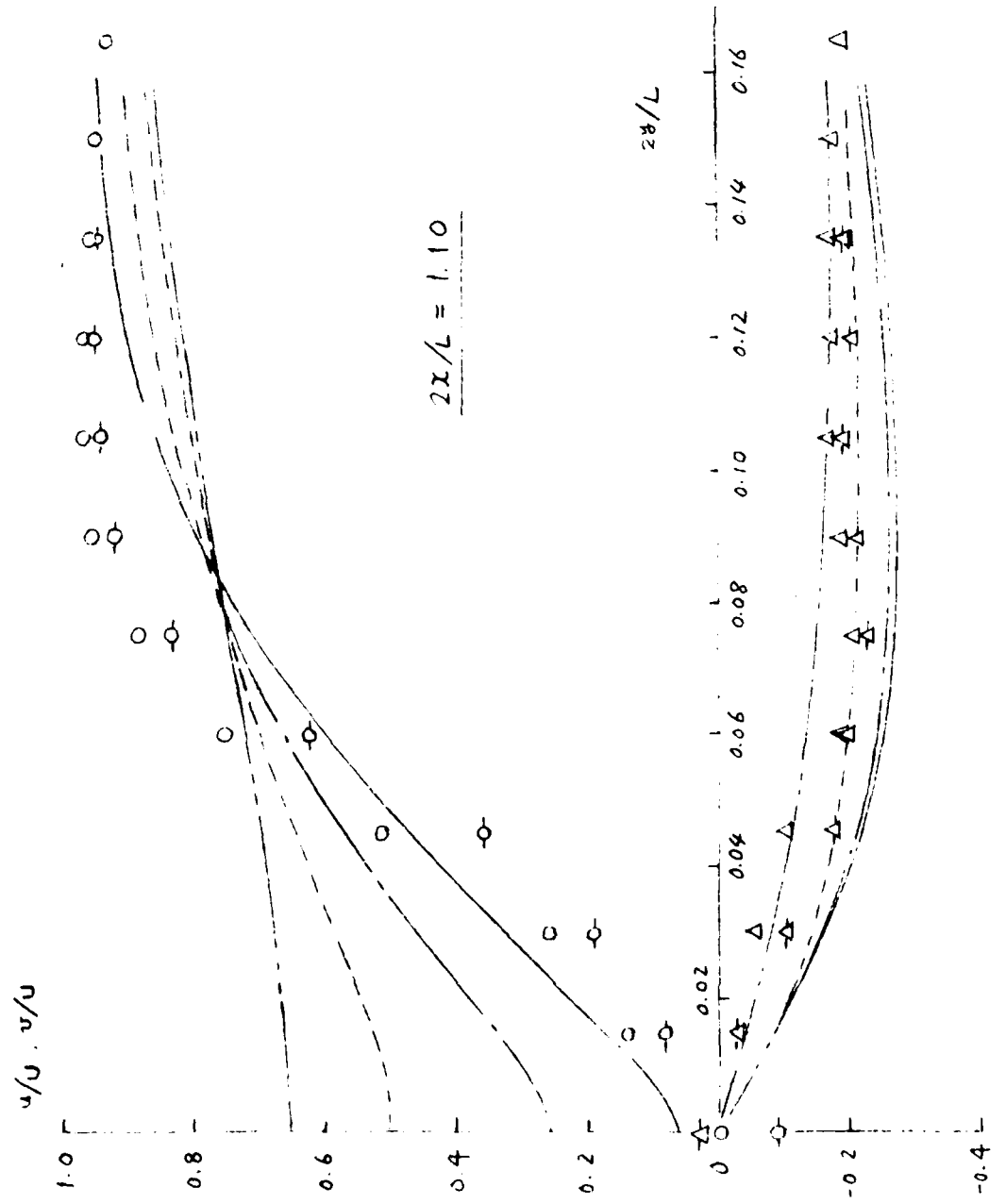

Fig. 10b Comparisons of Velocity Profiles (EM-[illegible])

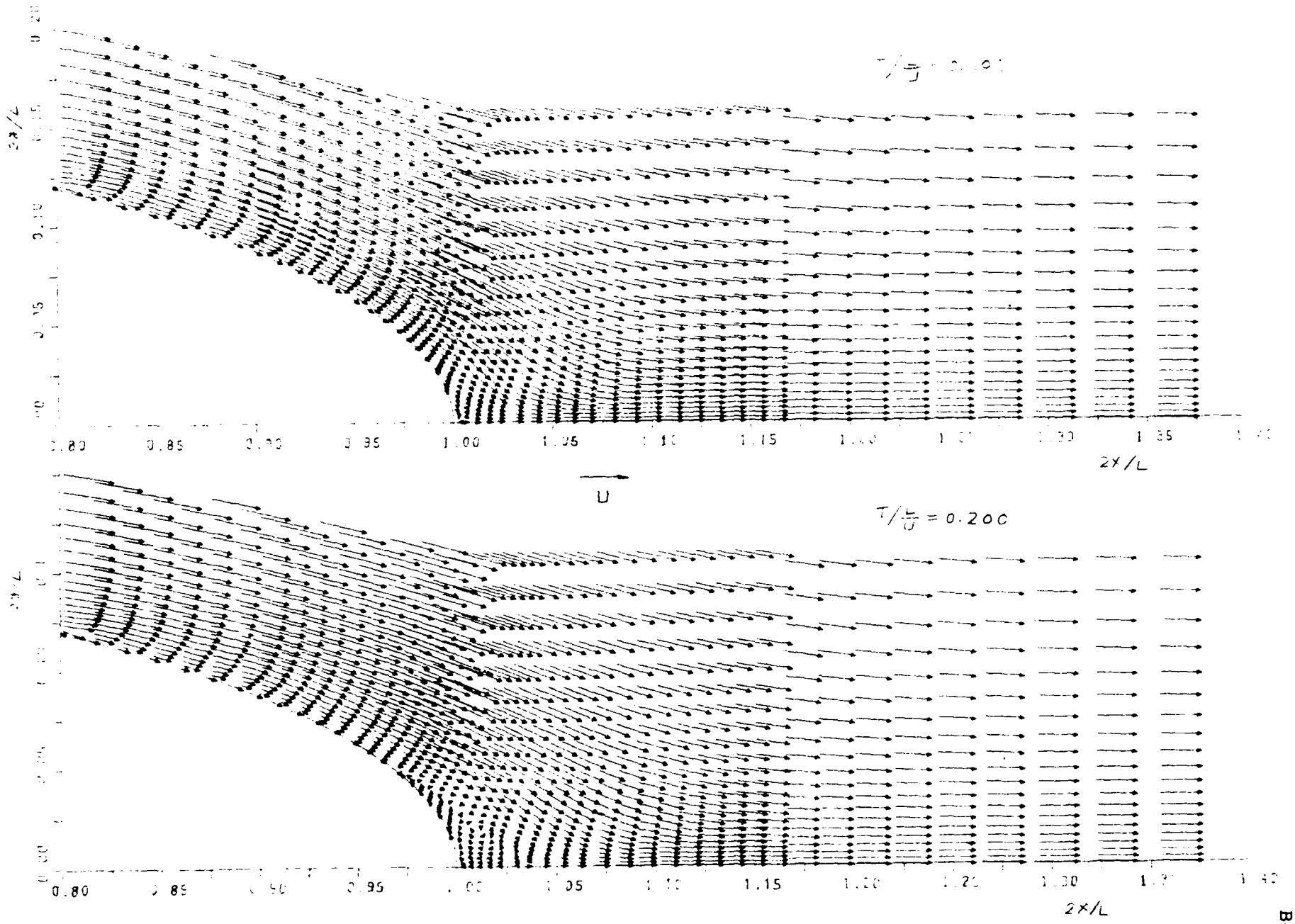

Fig.11a Calculated Flow Patterns (EM-200)

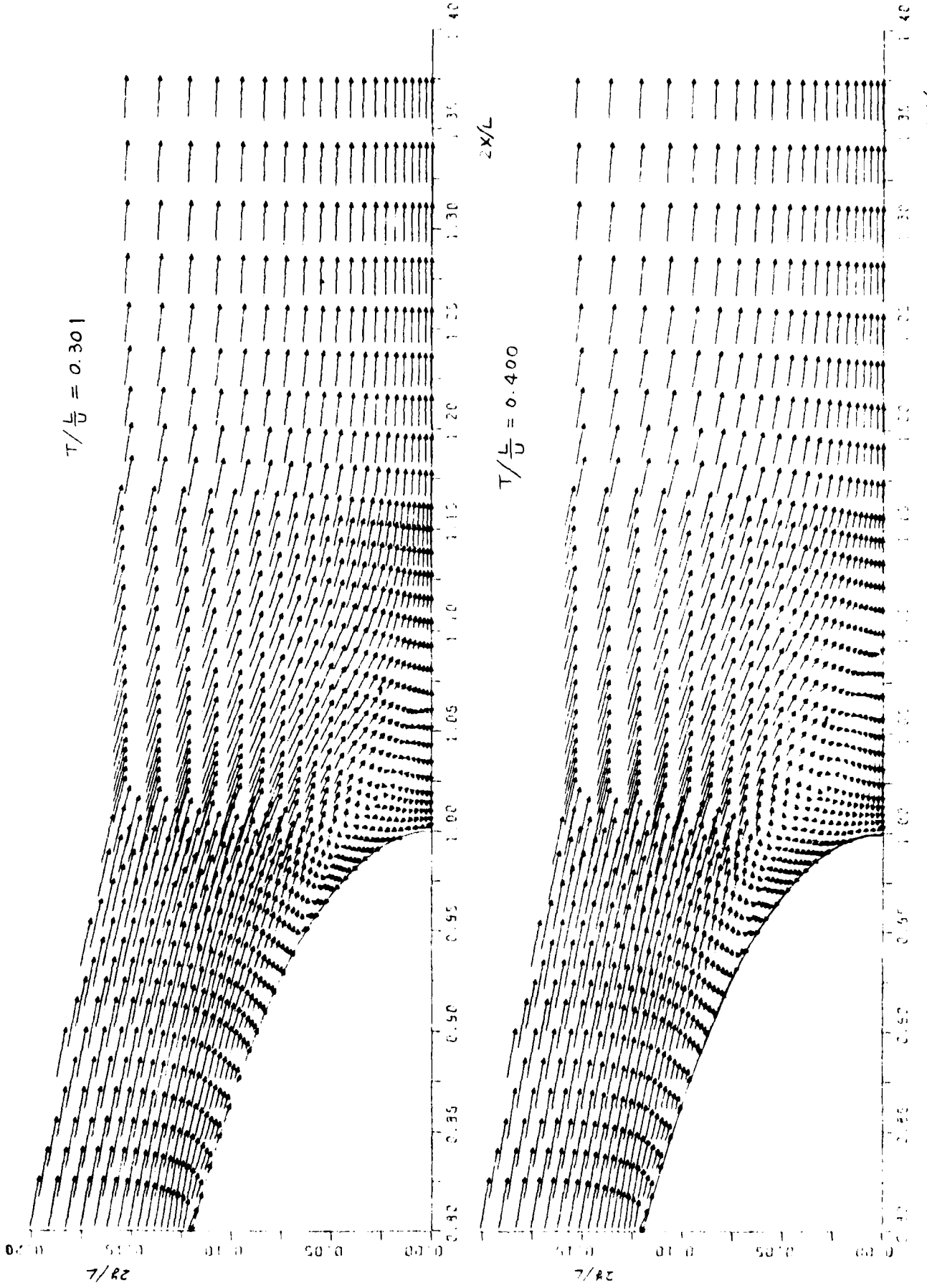

Fig.11b Calculated Flow Patterns (EV-200)

C. Free-Surface Boundary Layer and Necklace Vortex Formation

1. Introduction

The existence of a shear layer beneath a wavy free surface has been experimentally suggested; e.g., Takahama [1] and Longuet-Higgins [2]. Batchelor [3] gives a theoretical explanation for its development. The shear layer, which we shall call a free-surface boundary layer, develops due to the zero-shear-stress condition when the free surface has a significant curvature.

Besides the boundary layer on the hull and its accompanying wake, a free-surface boundary layer may also affect the ship wave resistance. The viscous effect of the free-surface boundary layer on wave resistance was discussed by Mori [4], where, by order-of-magnitude analysis, it was concluded that its effect might be less than those of the boundary layer on the hull and the wake, and only the latter was included in his calculation.

Recently, however, Kayo [5] has found that the presence of a free-surface shear layer, which is realized artificially in his research significantly affects the wave resistance.

In the first half of the present report, an attempt is made to give equations to predict the free-surface boundary layer in the 2-D case.

In the latter part, a theoretical explanation is made for the formation of the so-called necklace vortex around the bow. It is based on the drift theory (Lighthill [6]) or the vortex-stretching theory (Batchelor [7]). A similar idea has been introduced by Baba [8].

Through a simple calculation for the case of a vertical circular cylinder, it is demonstrated that even a slight vorticity in the incident flow can become very intense in the vicinity of the bow where flows are retarded, and that the observed effect of a bulbous bow on inhibiting the formaiton of this vortex can be explained by the acceleration of the flow near the free surface due to the presence of the bulb.

The combination of these two studies, which is left for a future investigation, may throw light on the bow-wave phenomena.

2. Free surface boundary layer equations

We limit ourselves here to the 2-D case. An orthogonal curvilinear coordinate system (s,n) is used together with the Cartesian coordinate (o-xyz) system, as shown in Fig. 1. The normal coordinate n consists of straight lines. u and w are the velocity components in s- and n-directions respectively.

The momentum equation in the s-direction is given by

$$u \frac{\partial u}{h \partial s} + w \frac{\partial u}{\partial n} + \kappa uw = - \frac{1}{\rho} \frac{\partial P}{h \partial s} - g \frac{\partial \zeta}{h \partial s} + \frac{1}{\rho} \left(\frac{\partial \sigma}{h \partial s} + \frac{\partial \tau}{\partial n} + 2\kappa\tau \right), \tag{1}$$

where h is the metric coefficient of the s-coordinate, P the pressure, ρ the density, and σ and τ are the normal stress and the tangential stress in s-direction respectively, including the Reynolds stresses. κ is the curvature of the s-coordinate defined by

$$\kappa = \frac{\partial h}{h \partial n} = \frac{d^2 \zeta}{dx^2} \left\{ 1 + \left(\frac{d\zeta}{dx} \right)^2 \right\}^{-3/2}. \tag{2}$$

The continuity equation is given by

$$\frac{\partial u}{h \partial s} + \frac{\partial w}{\partial n} + \kappa w = 0. \tag{3}$$

We assume that the related layer is so thin that the pressure is equal to the constant atmospheric pressure and that the derivative with respect to s is smaller than that with respect to n. Then Eq. (1) can be approximated by

$$u \frac{\partial u}{h \partial s} + w \frac{\partial u}{\partial n} + \kappa uw = -g \frac{\partial \zeta}{h \partial s} + \frac{1}{\rho} \left(\frac{\partial \tau}{\partial n} + 2\kappa\tau \right), \tag{4}$$

where ζ is the free surface elevation whose gradient is written in the steady case as

$$g \frac{d\zeta}{ds} + q \frac{dq}{ds} = 0, \tag{5}$$

where q is the potential velocity.

The boundary conditions on the free surface and at the edge of the boundary layer are as follows:

$$n = 0 \qquad \tau = 0, \tag{6}$$

$$n = \delta \qquad \omega = 0, \quad u = q, \tag{7}$$

where ω is the vorticity defined by

$$\omega = \frac{\partial u}{\partial n} + \kappa u - \frac{\partial w}{h \partial s}. \tag{8}$$

We assume that the Reynolds stresses are given in exactly the same form as the stresses due to the molecular viscosity in terms of velocity gradient. Then τ is given by

$$\tau = \mu_e \left(\frac{\partial u}{\partial n} - \kappa u + \frac{\partial w}{h \partial s}\right), \tag{9}$$

where μ_e is the equivalent viscosity coefficient.

If the flow is inviscid, the boundary condition of Eq. (6) is automatically satisfied and no boundary layers develop. If the flow is viscous, however, Eq. (6) yields an additional free-surface condition

$$\frac{\partial u}{\partial n} - \kappa u = 0 \quad , \qquad n = 0 \tag{10}$$

which is the source of a possible development of the free-surface boundary layer; the substitution of Eq. (10) into Eq. (8) gives the vorticity on the free surface;

$$\omega = 2\kappa u \quad , \qquad n = 0 \tag{11}$$

which is not zero unless κ is zero. This means that the vorticity is not zero on a curved free surface and a boundary layer possibly exists. It should be remembered that, if the free surface is flat, the boundary condition of Eq. (10) is automatically satisfied.

In the present paper, an integral method is used and the ordinary boundary-layer approximations are invoked. The third terms on l.h.s's of Eqs. (3) and (4) are omitted, and κ is assumed constant across the boundary layer and equal to the free-surface curvature.

The integration of Eq. (4) with respect to n yields

$$\frac{d\theta}{hds} + (2\theta + \delta^*)\frac{1}{q}\frac{dq}{hds} = -\frac{1}{\rho q^2}\tau\Big|_{n=\delta} - \frac{2\kappa}{\rho q^2}\int_0^\delta \tau dn, \tag{12}$$

where θ and δ^* are the momentum thickness and the displacement thickness respectively, defined by

$$q^2\theta = \int_0^\delta u(q-u)dn\ , \qquad q\delta^* = \int_0^\delta (q-u)dn. \tag{13}$$

In the derivation of Eq. (12), we have used Eqs. (3) and (5).

After neglecting the third term of Eq. (9), its substitution into Eq. (12) yields

$$\frac{d\theta}{hds} + (2\theta + \delta^*)\frac{1}{q}\frac{dq}{hds} = -\frac{\nu_e}{q^2}\{\frac{\partial u}{\partial n}\Big|_{n=\delta} + \kappa\ (q - 2q_o)\}, \tag{14}$$

where q_o is the velocity on the free surface.

If Eq. (8) can be approximated as

$$\omega = \frac{\partial u}{\partial n} + \kappa u = 0 \tag{15}$$

at $n = \delta$, the r.h.s. of Eq. (14) can be simplified to

$$\frac{d\theta}{hds} + (2\theta + \delta^*)\frac{1}{q}\frac{dq}{hds} = 2\nu_e\kappa\frac{q_o}{q}. \tag{16}$$

As a second equation, we use the entrainment equation*) which is obtained by an integration of Eq. (3),

$$\frac{d}{hds}(H_E\theta) + H_E\theta\frac{1}{q}\frac{dq}{hds} = E, \tag{17}$$

where

$$H_E = \frac{\delta-\delta^*}{\theta}\ ,$$
$$E = \frac{d\delta}{hds} - \frac{1}{q}w\Big|_\delta. \tag{18}$$

*)Of course, we can use an alternative equation such as the moment of moment equation. The choice of the best one is left for future work.

The entrainment function E is given apriori as a function of H_E.

Now we express the velocity profile in the boundary layer by a polynomial summation

$$u/q = a_o + a_1(\frac{n}{\delta}) + a_2(\frac{n}{\delta})^2 + a_3(\frac{n}{\delta})^3 \tag{20}$$

Then the boundary conditions Eqs. (6) and (7) give

$$\begin{aligned} a_1 &= ka_o, \\ a_2 &= -a_o(2k + 3) + k + 3, \\ a_3 &= (a_o-1)(k + 2), \end{aligned} \tag{21}$$

where $k = \kappa\delta$; the approximation of Eq. (15) is also invoked. Then δ^* and θ are written in terms of a_o and k as

$$\begin{aligned} \delta^*/\delta &= -\frac{1}{12}\{a_o(k + 6) + (k-6)\}, \\ \theta/\delta &= -\frac{1}{840}\{8a_o^2(k^2 + 11k + 39) + 2a_o(6k^2 + 17k - 102) \\ &\qquad + 8k^2 + 18k - 108)\}. \end{aligned} \tag{22}$$

Once θ and H_E have been obtained at a certain position by solving Eqs. (16) and (17), then a_o and k can be determined from Eqs. (18) and (22).

Thus we can calculate the free-surface boundary-layer flow. Further we can include it as one of the double-hull velocity components in the Rankine source method (see part A).

Formation of necklace vortex

We assume that the necklac vortex around the bow is formed by an accumulation of the vorticity generated in the free-surface boundary layer. As the drift theory suggests [6], because of the stretching of the streamlines around the bow, even a slight vorticity can form such an intensive vortex as is observed.

In the inviscid fluid, a vortex tube moves with a fluid particle and its strength remains constant (Helmholtz's theorem). This theorem gives a relation

$$\frac{\omega(t + \Delta t)}{|\omega(t)|} = \frac{\ell(t + \Delta t)}{|\ell(t)|} , \tag{23}$$

where ℓ is a material element parallel to the vorticity ω [7], and t is time.

To solve Eq. (23) is equivalent to solving the vorticity transport equation with the viscous diffusion term neglected.

If the vorticity can be assumed to be distributed on the $z = 0$ plane, the induced velocity is given by

$$u_v = \frac{1}{2} \omega_x \delta ,$$

$$v_v = - \frac{1}{2} \omega_x \delta , \tag{24}$$

$$w_v = - \frac{1}{4\pi} \iint \frac{\delta}{r^3} \{(x - x')\omega_y - (y - y')\omega_x\} \, dx' \, dy' ,$$

where $r^2 = (x - x')^2 + (y - y')^2$, ω_x and ω_y are x-, and y- components of ω respectively. δ is the nonzero vorticity layer. Here we assume that the vorticity is constant in the z-direction within the layer.

The velocity given by Eq. (24) can be included in q_v in the Rankine source method (see Part A), and we can calculate the free-surface elevation including the effect of a necklace vortex.

By making use of the relation

$$g \nabla \delta H = \omega \times \mathbf{q}, \tag{25}$$

we obtain the headloss δH as

$$g \delta H = \int_{x_o}^{x} \omega_y \, w dx \tag{26}$$

In Eq. (26), x_o is a far-upstream position where the head loss is zero.

4. A Numerical example for a vertical cylinder

When a vertical cylinder is in a uniform flow U, the velocity field is given by

$$u = U - Ua^2 \frac{x^2 - y^2}{r^4}, \qquad v = -2Ua^2 \frac{xy}{r^4}, \tag{27}$$

where a is the radius of the cylinder.

Fig. 2 shows the free-surface elevation along the centerplane (y = 0) which is approximately obtained by making use of Bernoulli's formula (the kinematic condition is not satisfied). The measurement was carried out with a point gauge. Agreement is good except near the bow. Just in front of the bow, a vortical motion can be observed. Around x/a = -2.1, a sudden increment in the surface elevation, which seems to form a wave-front line, is seen.

Fig. 3 shows the paths of fluid material particles, obtained by

$$x + iy = x_0 + iy_0 + \int_0^t (u + iv)\, dt, \tag{28}$$

where (x_0, y_0) is the initial position of a particle along which a vortex tube is initially assumed. In our present calculation, it is chosen at x/a = -1.9. The initial value of vorticity is determined by Eq. (11) as $|\omega_0| = 1.0$.

The solid lines show streamlines, the broken lines the positions of particles at the related time. It can be observed that vortex tubes are greatly stretched in the vicinity of the cylinder.

Fig. 4 shows the equivorticity contours; Fig. 4a and Fig. 4b show those of ω_x and ω_y respectively. In front of the cylinder, ω_y has increased more than seven-times its original intensity. This accumulation may explain the existence of the experimentally observed vortical motion there.

The effect on the generation of the ω_x- component is drastic. Although the ω_x- component rarely exists along the initial distribution line, a significant vorticity is attained which may form the longitudinal vortex along the cylinder.

Such accumulations may possibly affect the velocity field. Fig. 5 shows the induced velocity due to the free-surface vorticity which is obtained from Eq. (24). δ is assigned a constant value of 0.02a over the whole domain which is roughly equal to 10% of the wave height. Although the values assigned in the present calculation are quite modest, the induced velocity is significant. The negative sign of u_v indicates that the induced velocity is backward. As seen in Fig. 5, a stagnation point, where the addition of u_v to u becomes zero, is realized around x/a = - 1.05. This may account for the observed vortical motion ahead of the bow, and possibly for the occurrence of wave breaking. An exact calculation of the free-surface elevation, including the induced velocity, is highly desirable.

In Fig. 5, the head loss, obtained from Eq. (26), is also shown. Although it does not always compensate all the discrepancies observed in Fig. 2, it may be enough to produce an increment in resistance.

It is well known that a bulbous bow reduces resistance even at a low Froude number. The reason is believed to be that bulbs improve the bow flow so as to inhibit secondary flows or vortex formation but this has not been clearly demonstrated. A simple attempt will now be made to shed light on this phenomenon by introducing a point doublet in front of the cylinder. A point doublet of moment strength 0.125 Ua^3 is submerged at (-1.5a, 0, -0.75a). The original flow field, given by Eq. (27), does not correspond to that of the circular cylinder any more; this is ignored.

Fig. 6 shows the paths of material particles. Due to the acceleration by the point doublet, the stretching of a material tube is greatly moderated. Fig. 7 shows the equivorticity contours; as observed, the accumulation of vorticity is much less than that without a doublet. The longitudinal vortex has been remarkably weakened. The induced velocity, shown in Fig. 5, is also much less.

These results show that bow bulbs play a role to make the accumulation of vorticity less. This fact may provide a possible guideline to hull-form design; bulbs should be designed in order for the free-surface flow (not the entire flow!) to be accelerated so as to avoid the intensification of the free-surface vorticity.

4. Concluding remarks

The boundary layer equations are derived and it is shown that a free-surface boundary layer can develop when a free surface has a significant curvature.

The calculations and experiments, which will provide basic data for this not-well-known problem, are being performed.

The simple theory of drift is applied to the free-surface vorticity. The formations of the necklace vortex and the longitudinal vortex along the hull have been demonstrated. A thorough computation to predict the free-surface elevation will be undertaken by combining the described procedures with Rankine source method.

References

1) Takahama, H.; On a Freak Wave, Master Thesis of Hiroshima University (1974).

2) Longuet - Higgins, M.S.; Breaking Waves, Proc of 10th Symposium on Naval Hydrodynamics (1974).

3) Batchelor, G.K.; An Introduction to Fluid Dynamics, Cambridge University Press (1970), pp. 364.

4) Mori, K.; Prediction of Viscous Effects on Wave Resistance of Ship in Framework of Low Speed Wave Resistance Theory, Mem. of the Faculty of Eng. Hiroshima Univ., Vol. 7, No. 1 (1979).

5) Kayo, Y. and Takekuma, K.; On the Free Surface Shear Flow Related to Bow Wave-Breaking of Full Ship Models, Journ. of the Soc. of Naval Arch. of Japan, Vol. 149 (1981).

6) Lighthill, M.J.; Drift, J.F.M. Vol. 1 (1956)

7) Batchelor, G.K.; ibid, pp. 273.

8) Baba, E.; Some Free-Surface Phenomena around Ships to be Challenged by Numerical Analysis, Proc. 3rd Intern. Conf. on Numerical Ship Hydrodynamics (1981).

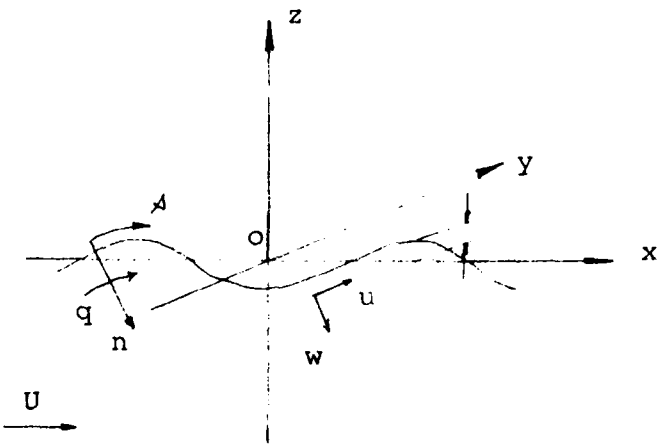

Fig. 1 Coordinate System

4. Concluding remarks

The boundary layer equations are derived and it is shown that a free-surface boundary layer can develop when a free surface has a significant curvature.

The calculations and experiments, which will provide basic data for this not-well-known problem, are being performed.

The simple theory of drift is applied to the free-surface vorticity. The formations of the necklace vortex and the longitudinal vortex along the hull have been demonstrated. A thorough computation to predict the free-surface elevation will be undertaken by combining the described procedures with Rankine source method.

References

1) Takahama, H.; On a Freak Wave, Master Thesis of Hiroshima University (1974).

2) Longuet - Higgins, M.S.; Breaking Waves, *Proc of 10th Symposium* on Naval Hydrodynamics (1974).

3) Batchelor, G.K.; An Introduction to Fluid Dynamics, Cambridge University Press (1970), pp. 364.

4) Mori, K.; Prediction of Viscous Effects on Wave Resistance of Ship in Framework of Low Speed Wave Resistance Theory, Mem. of the Faculty of Eng. Hiroshima Univ., Vol. 7, No. 1 (1979).

5) Kayo, Y. and Takekuma, K.; On the Free Surface Shear Flow Related to Bow Wave-Breaking of Full Ship Models, Journ. of the Soc. of Naval Arch. of Japan, Vol. 149 (1981).

6) Lighthill, M.J.; Drift, J.F.M. Vol. 1 (1956)

7) Batchelor, G.K.; ibid, pp. 273.

8) Baba, E.; Some Free-Surface Phenomena around Ships to be Challenged by Numerical Analysis, Proc. 3rd Intern. Conf. on Numerical Ship Hydrodynamics (1981).

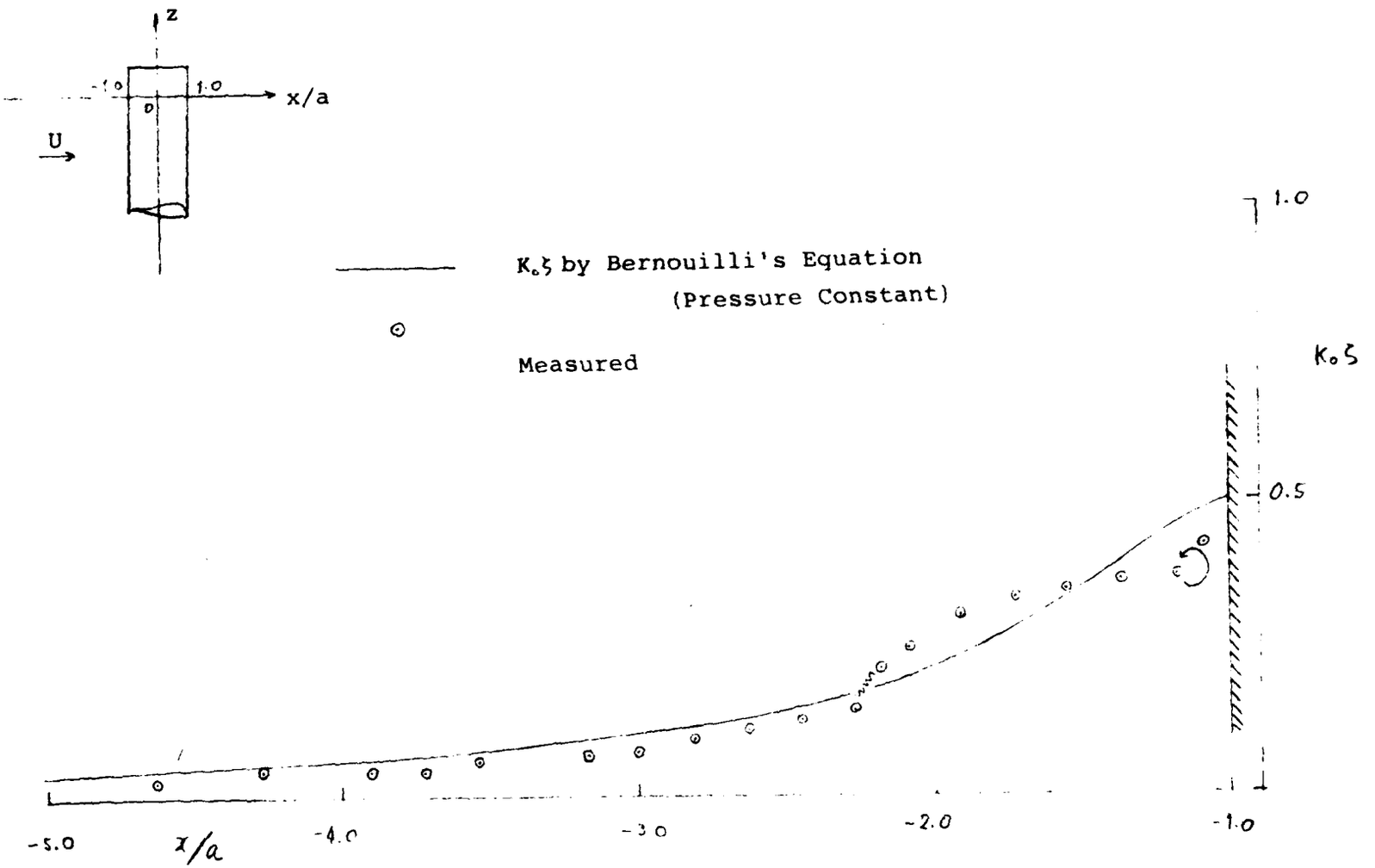

Fig. 2 Free Surface Elevation in front of Cylinder ($y=o$)

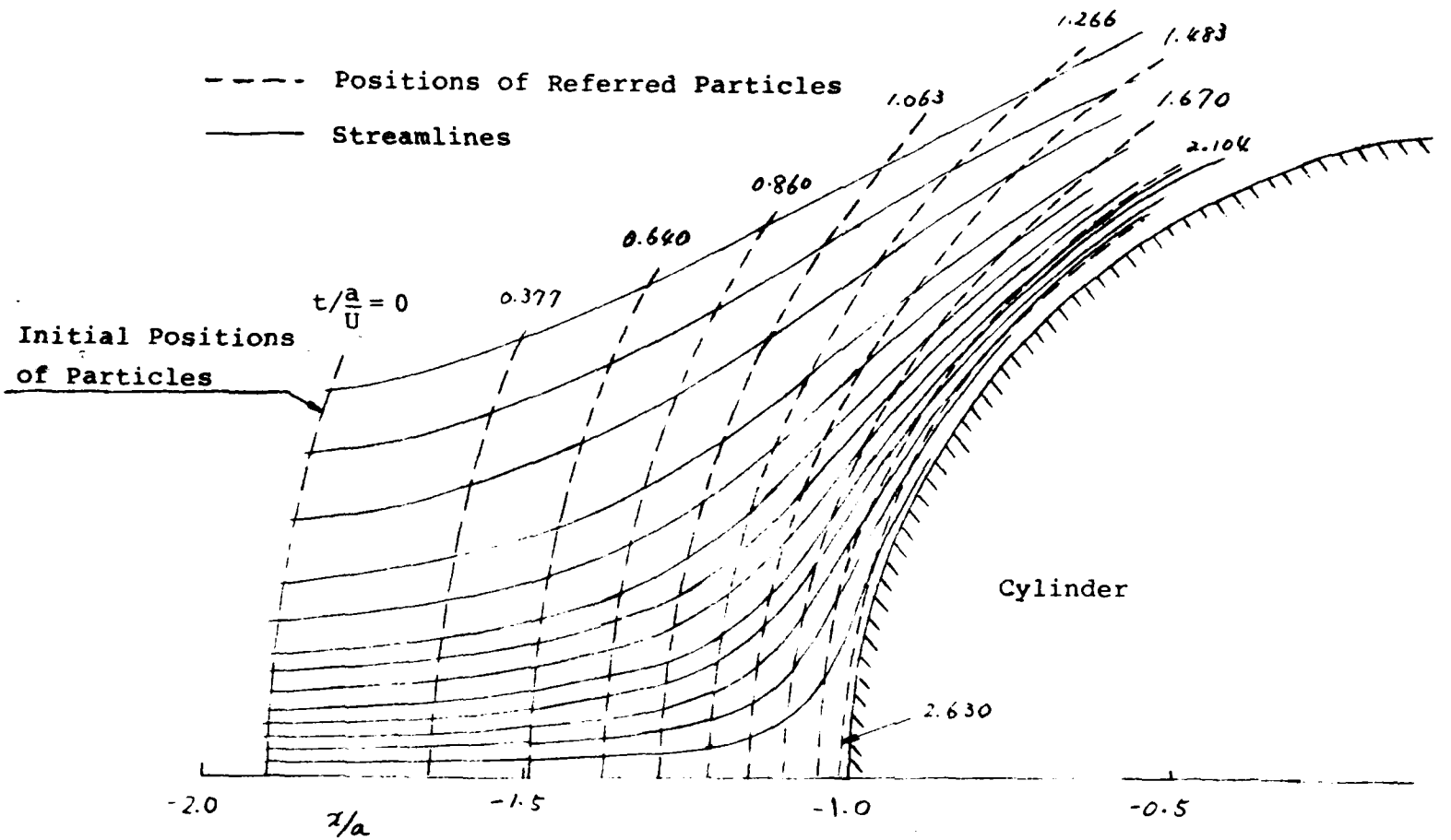

Fig. 3 Paths of Fluid Particles around Circular Cylinder

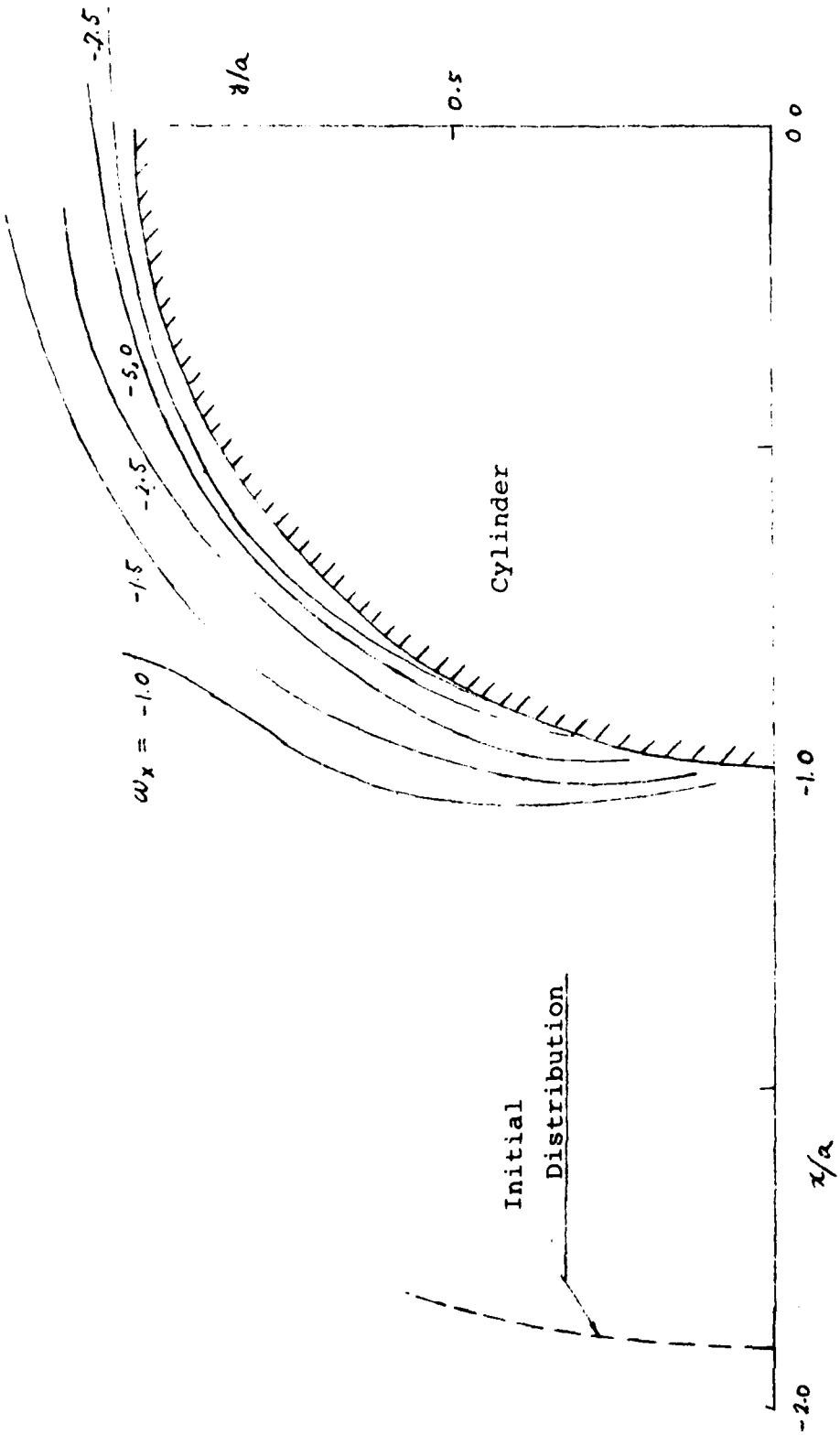

Fig. 4a Equi-Vorticity Contour around Cylinder (ω_x)

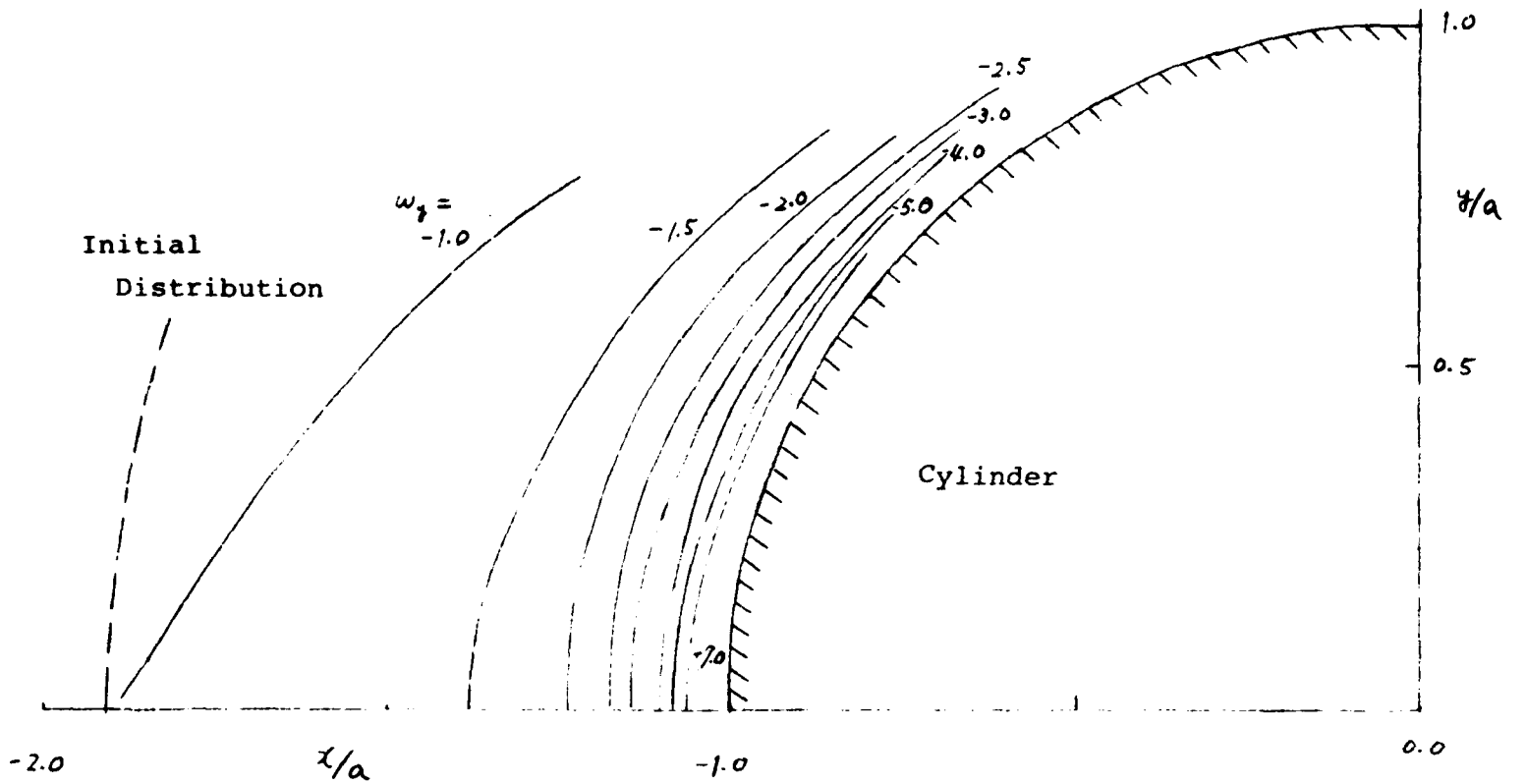

Fig. 4b Equi-Vorticity Contour around Cylinder (ω_y)

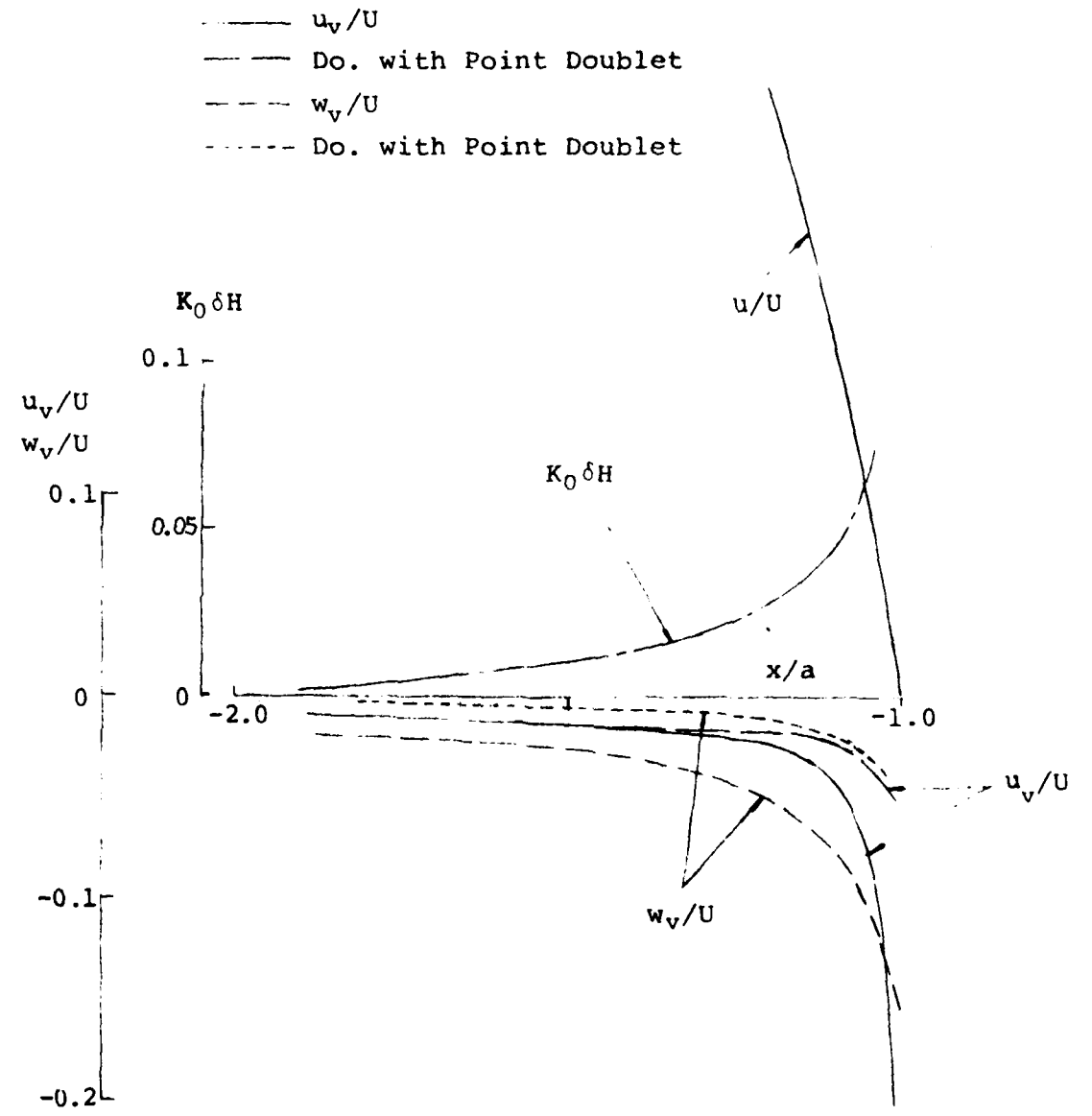

Fig. 5 Induced Velocity and Head Loss due to Free Surface Vorticity (y=0)

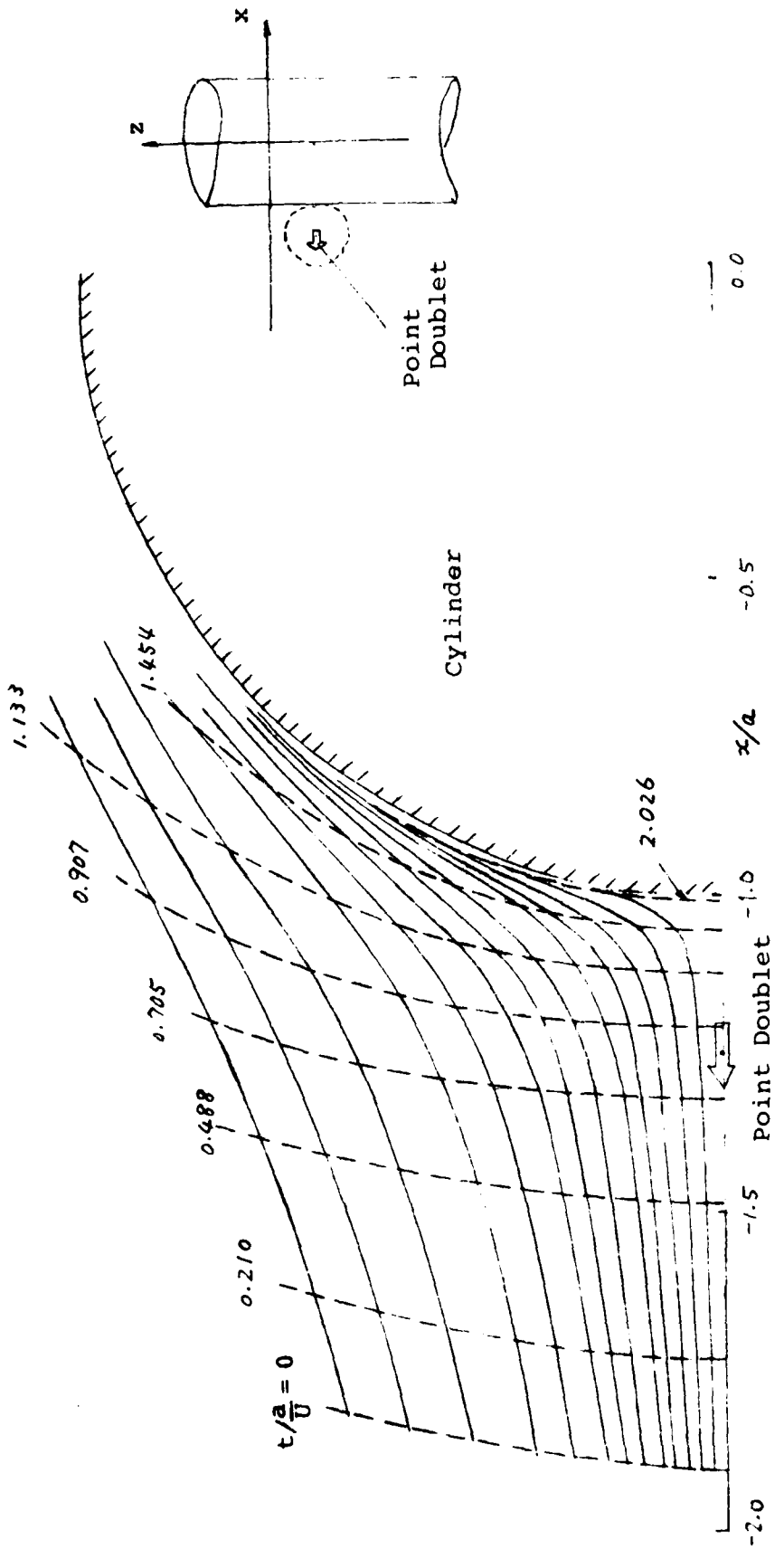

Fig. 6 Paths of Fluid Particles around Circular Cylinder with Submerged Point Doublet

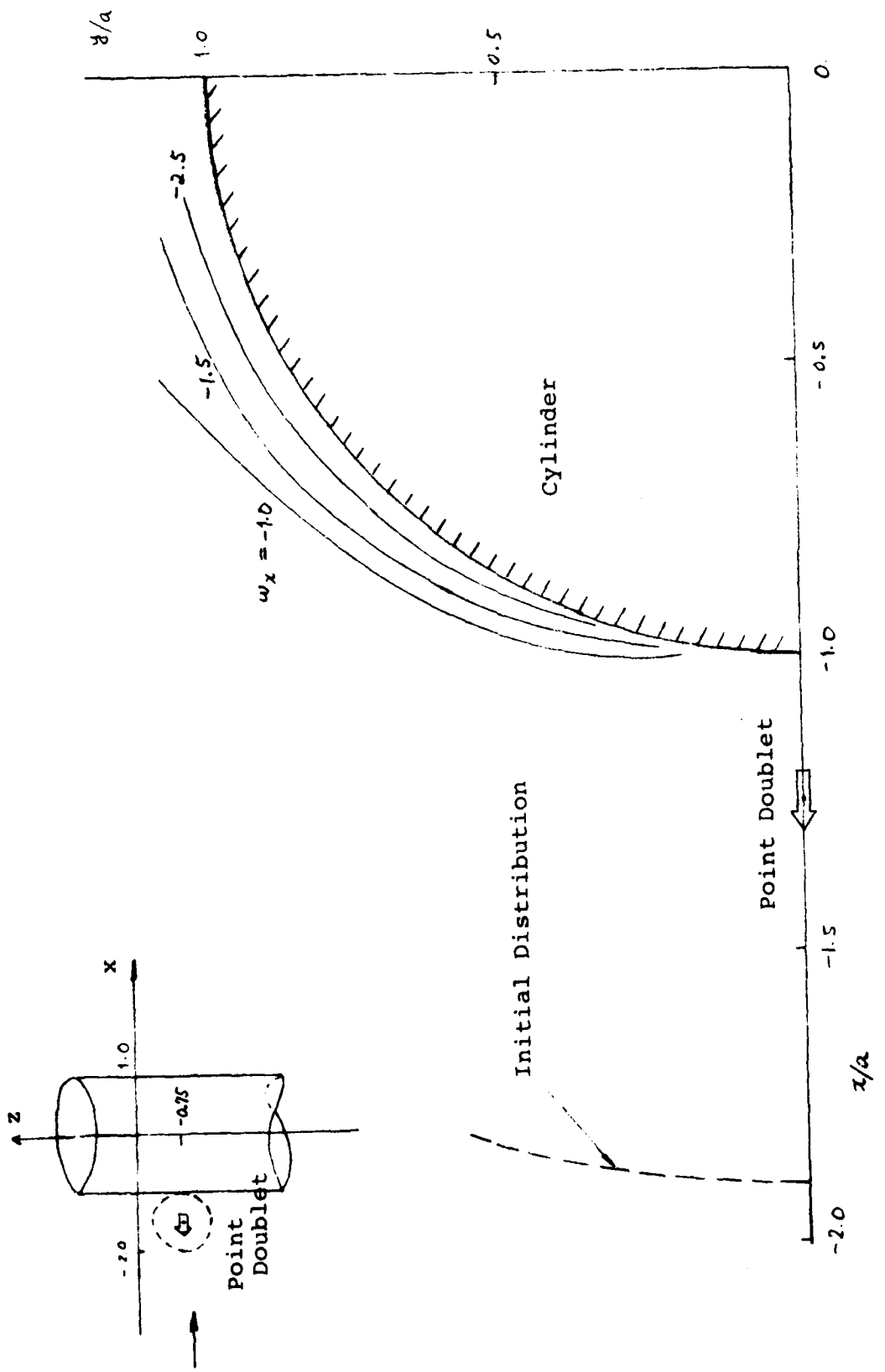

Fig. 7a Equi-Vorticity Contour around Cylinder with Submerged Point Doublet (ω_x)

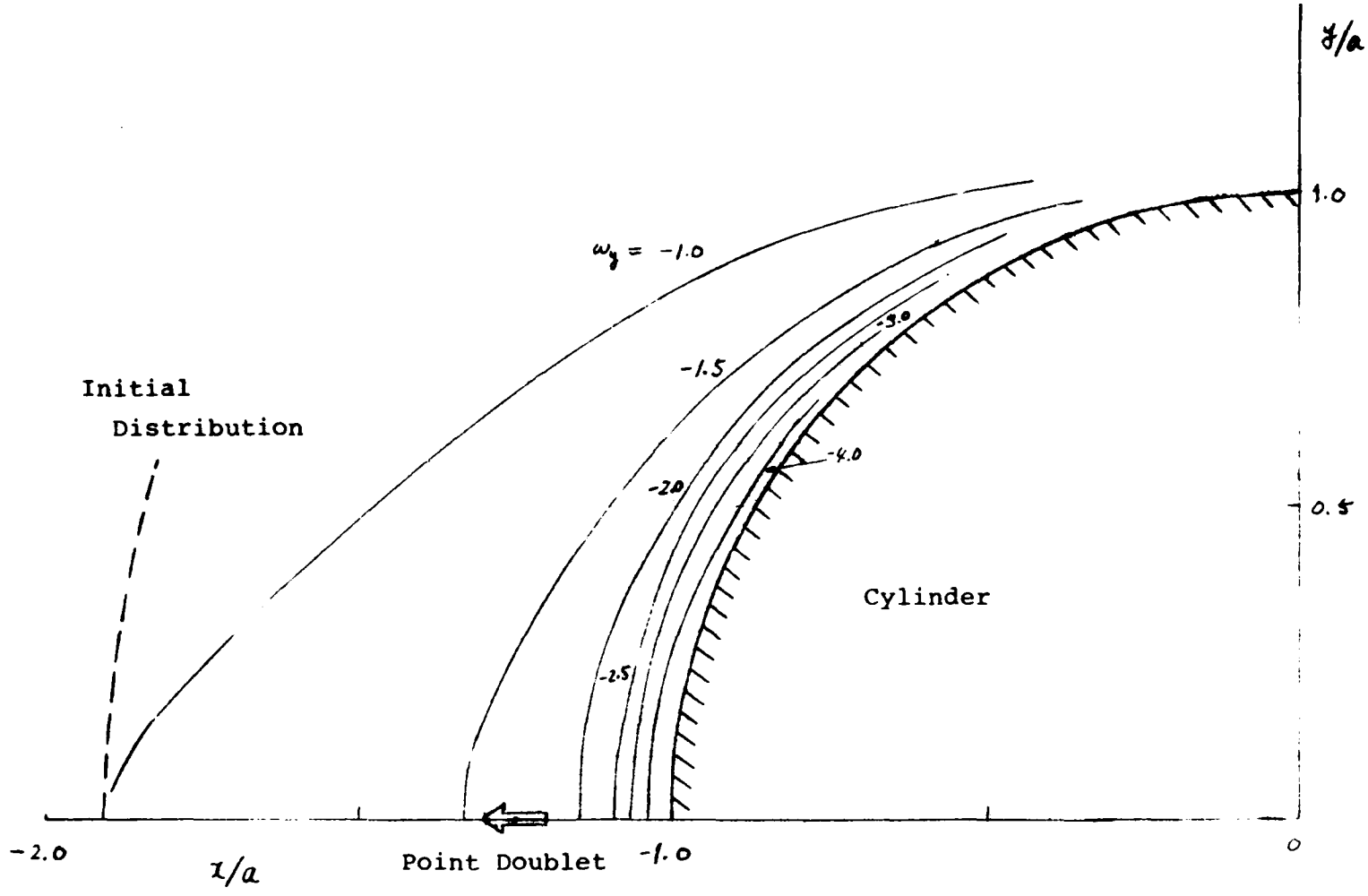

Fig. 7b Equi-Vorticity Contour around Cylinder with Submerged Point Doublet (ω_y)


DATE
ILME